




EX LIBRIS
UNIVERSITATIS
ALBERTENSIS

The Bruce Peel
Special Collections
Library



Digitized by the Internet Archive
in 2025 with funding from
University of Alberta Library

<https://archive.org/details/0162015205196>

University of Alberta

Library Release Form

Name of Author: Jinsong Wang

Title of Thesis: Thermodynamic automata simulations of fluid
flow and acoustic wave propagation

Degree: Master of Science

Year this Degree Granted: 2001

Permission is hereby granted to the University of Alberta Library to reproduce single copies of this thesis and to lend or sell such copies for private, scholarly or scientific research purposes only.

The author reserves all other publication and other rights in association with the copyright in the thesis, and except as herein before provided neither the thesis nor any substantial portion thereof may be printed or otherwise reproduced in any material form whatever without the author's prior written permission.

University of Alberta

**Thermodynamic automata simulations of fluid flow and
acoustic wave propagation**

by

Jinsong Wang



A thesis submitted to the Faculty of Graduate Studies and Research in partial fulfillment
of the requirements for the degree of Master of Science
in
Geophysics

Department of Physics

Edmonton, Alberta

Fall 2001

University of Alberta

Faculty of Graduate Studies and Research

The undersigned certify that they have read, and recommend to the Faculty of Graduate Studies and Research for acceptance, a thesis entitled **Thermodynamic automata simulations of fluid flow and acoustic wave propagation** submitted by **Jinsong Wang** in partial fulfillment of the requirements for the degree of Master of Science in Geophysics.

Abstract

In this study, a two-dimensional thermodynamic automaton model is reviewed and revised to simulate fluid flow in porous media. Unlike traditional lattice gas models based on a triangular or hexagonal cell, the thermodynamic automaton model is shape independent because it applies probabilistic collision rules. Therefore, a square lattice has been used in two dimensions and a cubic lattice in three dimensions. Temperature and isotropy are naturally maintained in this square model. The simulation results have been verified with theoretical predictions. The three-dimensional thermodynamic automaton model has been used to model both thermal equilibrium state and Darcy flow. Isotropy and temperature remain the internal properties of the model. Simulations of the barometric formula and diffusion in different media indicate that the cubic automaton model can be taken as a useful tool for the study of three-dimensional hydrodynamics.

Acknowledgements

I would first like to thank Dr. T. J. T. Spanos for his supervision, guidance, support and encouragement during the course of my research. His suggestions and valuable insight have been important contributions to this thesis.

Sincere thanks to Dr. Norman Udey for his introductory lecture about the automaton model and programming in C. This work would have been more difficult without his assistance and discussions.

I would also like to thank all the professors and graduate students in the geophysics group who have made my stay here more meaningful and enjoyable. Needless to say, I would also like to express my gratitude to Lynn Chandler who has worked hard for the benefit of the graduate students in our department.

Appreciations are given to the help of Robert Zschuppe and Marko Mah in proof-reading this thesis. Also, I am grateful to Robert Zschuppe for his correction of my english during daily conversations.

Special thanks are given to James MacKinnon for his technical support on the computer.

Finally, I would like to express my gratitude to my wife and my daughter for their love, support and understanding during my studies.

Table of contents

1	Evolution of cellular automaton from lattice gas method to thermodynamic automaton	1
1.1	Introduction	1
1.1.1	The notion of automata	1
1.1.2	Literature review	3
1.2	Evolution of the cellular automata for modelling hydrodynamic Processes	7
1.2.1	Lattice gas automata and hydrodynamics	7
1.2.2	Different models	9
1.2.3	Two approaches to Navier-Stoke equation	13
1.3	Outline of the following chapters	17
2	Construction of a thermodynamic automaton model	18
3	Applications of 2D thermodynamic automata	21
3.1	Introduction	21
3.2	Modelling particle number distribution due to gravity.....	21
3.2.1	Theoretical background	21
3.2.2	Model and simulation results	22
3.3	Laminar flow, turbulence and Reynolds number	25
3.3.1	Theoretical background	25
3.3.2	Models and numerical simulations	26

3.4	Heat convection	32
3.4.1	Theoretical background	32
3.4.2	Models and numerical simulations	33
3.5	Diffusion and dispersion in porous media using tubes model	37
3.5.1	Theoretical background	37
3.5.2	Models and simulation results	40
3.5.3	Concluding remarks	48
3.6	Wave propagation in porous media	49
3.6.1	Introduction	49
3.6.2	Theoretical background	50
3.6.3	Numerical model and simulation results	59
3.7	Summary	54
4	Implementation of 3D thermodynamic automata	55
4.1	Introduction	55
4.2	Construction of 3D thermodynamic automata	56
4.2.1	Three dimensional coordinate systems (cubic, sphere)	56
4.2.2	Collision, propagation and motion rules	57
4.2.3	Boundary conditions	58
4.2.4	Codes revision	59
5	Applications of 3D thermodynamic automaton simulation	60
5.1	Introduction	60
5.2	3D thermodynamic automata simulation of thermal equilibrium state	60
5.2.1	Theoretical background	60
5.2.2	Models and simulation results	62

5.3	3D thermodynamic automaton simulation of Poiseuille flow and Darcy flow	66
5.3.1	Theoretical background	66
5.3.2	Models and simulation results	66
5.4	3D thermodynamic automaton simulation of particle number distribution due to gravity	70
5.4.1	Theoretical background	70
5.4.2	Models and simulation results	70
5.5	3D thermodynamic automaton simulation of diffusion in porous media	72
5.5.1	Theoretical background	72
5.5.2	Models and simulation results	73
5.5.3	Concluding remarks	83
5.6	Summary	83

6	Summary, conclusions and recommendations	84
----------	---	-----------

	Bibliography	86
--	---------------------	-----------

List of Figures

Figure 2.1	Diagram of XY coordinates for the motion of the particles	19
Figure 3.1	Simulation of 2D gas distribution due to gravity	23
Figure 3.2	Plot of natural logarithm of Gas number distribution at different time steps.....	24
Figure 3.3	Plot of natural logarithm of Gas number distribution at time steps 4000 and 5000.....	24
Figure 3.4	Diagram of the velocity vectors for laminar flow (a), and turbulent flow (b)	26
Figure 3.5	Particle velocity in the x direction, determined by averaging along each row for laminar flow (pressure drop=0.00001).....	27
Figure 3.6	Particle velocity in the x direction, determined by averaging along each row for turbulence (pressure drop=0.0001)	28
Figure 3.7	Particle velocity in the y direction, determined by averaging along each row for laminar flow (pressure drop=0.00001)	28
Figure 3.8	Particle velocity in the y direction, determined by averaging along each row for turbulence (pressure drop=0.0001)	29
Figure 3.9 (a)	Particle velocity vectors for the onset of turbulence, columns 1 to 20	29
Figure 3.9 (b)	Particle Velocity vectors for the onset of turbulence, columns 21 to 40...	30
Figure 3.9 (c)	Particle Velocity vectors for the onset of turbulence, columns 41 to 60...	30
Figure 3.9 (d)	Particle Velocity vectors for the onset of turbulence, columns 61 to 80...	31
Figure 3.9 (e)	Particle Velocity vectors for the onset of turbulence, columns 81 to 100...	31
Figure 3.10	Particle velocity vectors at an equilibrium state before heating, columns 1 to 20	34
Figure 3.11	Particle velocity vectors at an equilibrium state after heating, columns 1 to 20 after 5000 time steps	34
Figure 3.12	Particle velocity vectors at an equilibrium state before heating, columns 60 to 80	35

Figure 3.13	Particle velocity vectors at an equilibrium state after heating, columns 60 to 80 after 5000 time steps	35
Figure 3.14	Particle velocity vectors at an equilibrium state before heating, columns 80 to 100	36
Figure 3.15	Particle velocity vectors at an equilibrium state after heating, columns 80 to 100 after 5000 time steps	36
Figure 3.16	Schematic diagrams of tube models	41
Figure 3.17	Diffusion in a homogeneous porous medium (average of all tubes)	42
Figure 3.18	Diffusion in a heterogeneous porous medium (average of all tubes)	43
Figure 3.19	Diffusion in a homogeneous porous medium (specific tube averages).....	43
Figure 3.20	Diffusion in a heterogeneous porous medium (specific tube averages)....	44
Figure 3.21	Comparison of diffusion in homogeneous and heterogeneous porous media (average of all tubes)	44
Figure 3.22	Dispersion in a homogeneous medium with a different pressure drop	45
Figure 3.23	Dispersion in a homogeneous porous medium (average of all tubes)	45
Figure 3.24	Dispersion in a heterogeneous porous medium (average of all tubes)	46
Figure 3.25	Comparison of dispersion in homogeneous and in heterogeneous media (average of all tubes)	46
Figure 3.26	Dispersion in a homogeneous medium (specific tube averages)	47
Figure 3.27	Dispersion in a heterogeneous medium (specific tube averages)	47
Figure 3.28	Lattice gas automaton simulation results of acoustic wave propagation (amplitude versus time at different offset).....	52
Figure 3.29	Lattice gas automaton simulation results of acoustic wave propagation (amplitude versus position at different time steps).....	52
Figure 3.30	Diagram of common source and receivers configurations	53
Figure 3.31	Lattice gas automaton simulation of acoustic common shot point gather collected according to Figure 3.30	53
Figure 4.1	Diagram of the spherical coordinate system used in the 3D thermodynamic automata model	56
Figure 4.2	Diagram of particles hitting left and top boundaries	58

Figure 5.1	The initial simulation particle speed. Each particle has the same mass and speed $v=0.1$ or $v=0.2$ in two models respectively	63
Figure 5.2	The particle speed distributions after 1000 iterations	63
Figure 5.3	Corresponding plots of $\ln(P(E))$ versus energy E for the particle speed distribution with $v=0.1$ and 0.2	64
Figure 5.4	Sample plot of probability density of particles versus speed and vertical angle α . Selected section is obtained when horizontal angle θ equals 50°	64
Figure 5.5	Sample plot of probability density of particles versus speed and horizontal angle θ . Selected section is obtained when vertical angle α equals 50°	65
Figure 5.6	Velocity profile of Darcy flow at yz cross section obtained from the 3D lattice gas simulation after 5000 time steps	69
Figure 5.7	Velocity profile of Poiseuille flow at yz cross section obtained from the 3D lattice gas simulation	69
Figure 5.8	3D thermodynamic automaton simulation of the Barometric formula. Cross-section of the xz plane at $y=5$	71
Figure 5.9	3D thermodynamic automaton simulation of the Barometric formula. Cross-section of the xy plane at $z=5$	71
Figure 5.10	Analytic solution to the evolution of concentration c using Mathematica for the given values of the parameter Dt	73
Figure 5.11	3D modelling of the diffusion process in a tube with periodic boundary conditions. Tracing particles are arranged into right part of the cubic tube	76
Figure 5.12	3D modelling of the diffusion process in a tube with thermodynamic boundary conditions. Tracing particles are arranged into right part of the cubic tube.....	77
Figure 5.13	3D modelling of the diffusion process in a tube with periodic boundary conditions. Tracing particles are arranged into middle part of the cubic tube along the x -axis direction.	78

Figure 5.14	3D modelling of the diffusion process in homogeneous porous media with periodic boundary conditions.....	79
Figure 5.15	3D modelling of the diffusion process in heterogeneous porous media with periodic boundary conditions	80
Figure 5.16	Comparisons of diffusion processes in tube, homogeneous porous media and heterogeneous porous media	81
Figure 5.17 (a)	Porosity structure in the heterogeneous porous media in cross-section xy at $z=1$	82
Figure 5.17 (b)	Porosity structure in the heterogeneous porous media in cross-section xy at $z=2$	82

List of tables

Table 1 Reynolds number of laminar flow and the onset of turbulent flow 32

Chapter 1

Evolution of cellular automaton from lattice gas method to thermodynamic automaton

1.1 Introduction

1.1.1 The notion of automata

Automata theory was first proposed by John Von Neumann in the late 1940's (Neumann, 1966). In his book, the automata rules have been used as a systematic theory, which is mathematical and logical in form and characterized as self-reproducing. It provided an essential way to help in understanding natural systems (natural automata) as well as help understand both analog and digital computers (artificial automata). Similarly, the word "automata" has been applied to mathematical models of devices, which provide information by responding to certain inputs (Salomaa, 1969). Further study also showed that cellular automata are examples of mathematical systems conducted from many identical components, each of which is simple, but capable of modelling complex behavior when put together (Wolfram, 1984).

Definitions of automata were given by Weisbuch (1991). In his book, he defined the classical automata as the second discretization operation to replace the continuous variables and differential equations by finite state automata. A simplified automaton was defined from its sets of inputs and outputs and from a transition function, which gives the output at time $t+1$ as a function of the inputs and sometimes also the internal state at time t . A closer definition of automata given by the author is that: "Cellular automata are automata distributed on the nodes of a periodic lattice, a discrete geometrical structure, invariant under certain translation and rotation operations."

Cellular automata as a numerical simulation method can be considered to be systems of differential equations, which have been simplified by extreme discretization. They differ

from finite difference approximations in that space and time are discretized but dependent variables are continuous (Boghossian and Levermore, 1987).

A cellular automaton model is constructed by setting up a lattice of sites that have some connections with each other. The connectivity of each cell is limited to a certain neighborhood and the structure of this neighborhood preserves the translation and rotational symmetries of the lattices. Each cell contains a finite set of particles, to which special parameters are assigned. The particles of a particular cell evolve synchronously in discrete time steps. The further particle states are determined by the present states of its neighboring sites. Repeating the procedure above, the systems will evolve according to fundamental physical rules.

Since the advent of cellular automata, many automata systems have been made (Conway, 1982; Wolfram, 1986a; Travis et al., 1988; Succi, 1988; Toffoli, 1989; Appert et al., 1991; Segre and Deangeli, 1995; Udey et al., 1999). These systems have proven to be powerful tools in modelling dynamic systems in areas such as the physics of growth, biological science, computer science, physical chemistry, earth science and hydrodynamics. The systems make it possible to follow the interaction mechanisms between automata and observe the lattice state at any point in time. In these fields, the dynamical properties are usually expressed by partial differential equations with nonlinear terms that are not solvable by analytical methods. Classical methods are computationally intensive and require complicated programming techniques and large computer memory. The speed of computations, the simplicity of the programming involved, and the ability to directly visualize the evolution of patterns generated by these systems (interface, crystals, hydrodynamic structures, flame fronts, etc.) make cellular automata invaluable tools to provide solutions for nonlinear process with complicated boundaries, such as fluid flow through porous media.

1.1.2 Literature review

Productive work was done by Von Neumann on topics of “the general and logical theory and organization of complicated automata; probabilistic logics and synthesis of reliable organisms from unreliable components; the computer and the brain” before he successfully provided a self-reproduction cellular model for the behavior of complex systems (Neumann, 1966). Conway’s “Game of life” (1960) adopted the cellular automata techniques and made the word “cellular automata” very popular.

Later on, many researchers have focused on solving earth science simulation problems. Bak and Tang, (1989) used a simple cellular automaton stick-slip type model to analyze a self-organized critical phenomenon of earthquakes. Brown et al. (1991) also constructed a cellular automaton model of earthquakes. Lundquist et al. (1992) applied cellular automaton models to plate tectonics of continents on Earth and a purely oceanic-style lithosphere on Venus. Bean et al. (1993) adopted a high-dimensional, self-organized, critical cellular automaton to understand the behavior of seismic reflectivity in boreholes and its relationship to crystal deformation models. An and Sammis (1996) developed a 2D computer automaton model to simulate the growth and coalescence of a network of faults, leading to the formation of a large, through-going shear zone. Tipper (1997) modelled carbonate platform sedimentation using a cellular automaton. However, most studies have involved hydrodynamic simulations.

Hardy et al. (1976) first constructed an HPP lattice gas model for simulation of fluid flow in the hydrodynamic domain. Since then, a great deal of research has concentrated on fluid dynamics using cellular automata models. Wolfram (1984) used cellular automata for the description of mathematical systems. Later on, Wolfram (1986b) conducted a thorough study of the basic theory for cellular fluids. Frisch et al. (1986) showed that a class of deterministic lattice gases with discrete Boolean elements simulates the Navier-Stokes equation and can be used to design simple, massively parallel computing machines.

Lebowitz et al. (1986) described some recent progress in deriving autonomous hydrodynamic equations for macroscopic variables from modelling stochastic microscopic dynamics of particles on a lattice, which provided theories in support of automata. In 1987, Balasubramanian et al. introduced a lattice gas model for the Navier-Stokes equation and obtained Darcy flow. Binder (1987) described a lattice model for the study of the physical and dynamical Lorentz gas properties. Burgess et al. (1987) conducted research on buoyant mixtures of cellular automata gases. Many authors (Chen, 1987; D’Humières et al., 1985, 1986a, 1987; McCauley, 1987; Oono, 1987; Montgomery, 1987) contributed different aspects on cellular automata systems focused on hydrodynamics simulations.

Chen et al. (1988) presented a magneto hydrodynamic lattice gas model which was a direct extension of the lattice gas model for incompressible Navier-Stokes fluids. In this model, a bi-directional random walk process was used. Chopard (1988) employed a two-speed lattice gas to study heat propagation in a fluid at rest. A good agreement is found between analytical Boltzmann and thermo-hydrodynamic equations and numerical cellular automata simulations. Clavin et al. (1988) simulated free boundaries in flow systems by introducing two different types of particles that can react following a specific kinetic scheme based on autocatalytic reactions.

Boon and Noullez (1989) gave detailed identification rules for lattice gas diffusion. Such identification can be realized by introducing different types of particles and extending the cellular automata collision rules to include type conservation.

Demasi et al. (1989) investigated a stochastic version of cellular automata used for simulating hydrodynamic flows to HPP and FHP models. He stated in the paper that looking through a window in space-time one sees a kinetic behavior, described by a Boltzmann-like equation; looking through different lenses, focused on a longer time scale, one sees hydrodynamic behavior described by an Euler-like equation; focusing on still longer times and suitably choosing the initial state, one observes the analogue of the incompressible Navier-Stokes equation.

Rothman (1990) expanded the research to macroscopic laws for immiscible two-phase flow in porous media using a Galilean-invariant lattice model. The results showed that the macroscopic flow is a nonlinear function of the applied forces for sufficiently low levels of forcing, but linear thereafter.

Appert et al. (1991) adopted a triangular lattice model able to undergo a liquid-gas transition. The model is obtained by adding an attractive force to the FHP model in the form of non-local interactions. Gunstensen (1991) introduced a new lattice-gas model, which extended the two-phase immiscible lattice gas to the simulation of a mixture of three immiscible fluids.

Janecky (1992) proposed a lattice gas automaton for flow and transport in geochemical systems. Appert et al. (1992) carried out a study on simulating evaporation in porous media with the lattice gas method. Cheng and Ebner (1993) conducted a research based on an Ising lattice gas model for the dynamics of liquid-droplet spreading by using a Monte Carlo simulation method. Di et al. (1994) used interacting lattice gas-cellular automata to model water infiltration in unsaturated porous media. Huang (1995) added absorbing boundary and free-surface conditions to model wave propagation in lattice solid approaches. An absorbing boundary condition for these microscopic approaches has been designed by setting the microscopic reflection coefficients at the borders of a model to zero and adding viscous layers to the borders. Special interaction rules at the free surface are specified to take into account the effect of the free surface on quasi-particle movements. Jiao (1996) extended lattice gas automata methods to lattice Boltzmann methods as alternatives for modelling fluid dynamics and other systems described by partial differential equations. Waite et al. (1998) carried out a lattice gas automaton to study the effect of surface geometry on fracture permeability. Udey et al. (1999) constructed a thermodynamic automaton model using Lorentz invariant binary elastic collision rules. They associated with each particle a continuous momentum, which is used to control the motion of the particle on the lattice and to employ the temperature inside. Yang et al. (1999) presented a thermodynamic automaton model of fluid flow in porous media. He demonstrated that the nonrelativistic model could be used to accurately

simulate well-known results involving single-phase flow and diffusion in porous media. Kuentz et al. (2000) used a 2D lattice gas to calculate the effective electrical conductivity of saturated porous media as a function of porosity and conductivity ratio R between the pore-filling fluid and the solid matrix for various microscopic structure of the pore space.

Recent studies have also been advanced to 3D simulations of fluid flow based on FCHC cellular automata models. (D'Humières and Laliemand, 1986b; Molvig et al., 1989; Dubrulle et al., 1991; Gunstensen, 1991; Hénon, 1992; Steacy et al., 1995)

In summary, cellular automaton lattice gas models, have been applied to various hydrodynamic subjects, and have been recognized as a powerful tool in modelling fluid dynamics in porous media.

1.2 Evolution of the cellular automata for modelling hydrodynamic processes

1.2.1 Lattice gas automata and hydrodynamics

Lattice gas models, which are also called lattice gas automata, are a special class of cellular automata with particles initialized in cells on a lattice, for example triangular or square lattice. It was first introduced by Frisch, et al. (1986) as a tool to simulate the incompressible Navier-Stokes equation in the limit of a large lattice size and low particle velocity. Lattice gas automata have already played an important role for the study of hydrodynamics and systems governed by related partial differential equations (Holme et al., 1992). Because of its speed and simplicity, lattice gas hydrodynamics has recently received considerable attention. This method not only describes macroscopic phenomena using ensemble averages, but it also provides microscopic detail which is important for improving our understanding of volume-averaged parameters used in large scale simulations of flow through porous media (Chen et al., 1991).

Lattice gas models are sufficiently interesting and useful to be regarded separately (Boghossian, 1989). Various terminologies in the literature, such as cellular automata, lattice gas automata or lattice gas, have been used. However, these terminologies all referred to the same method of solving hydrodynamics problems (Yang, 1997).

One can use a lattice gas model to simulate fluid flow because both a gas and a liquid obey the Navier-Stokes equation. If a gas behaves in an incompressible fashion and the temperature is held constant, then both the gas and liquid's behavior is identical.

Lattice gas automata are an alternative to the use of differential equations. In fluid mechanics, the behavior of moving fluids is described by a nonlinear partial differential equation, the Navier-Stokes equation.

$$\frac{\partial \rho \mathbf{v}}{\partial t} + \nabla \cdot (\rho \mathbf{v} \mathbf{v}) = -\nabla p + \nabla (\mu \nabla \mathbf{v}) + \rho \mathbf{f} \quad (1.1)$$

where ρ is the local density of the medium, \mathbf{v} is the average velocity, μ is the shear viscosity, \mathbf{f} is a body force, t is the time.

With small velocities, in the linear regime (laminar flow), one can linearize this equation and solve it without much difficulty. However, if the velocities are large, instabilities appear and analytical methods can no longer be used. The Navier-Stokes equation is based on a macroscopic description of physical quantities. It depends on the velocities of the volume elements of the fluid. The Navier-Stokes equation is simulated by first discretizing and representing space as a cellular lattice. For the fluids, the particles are required that move at a certain velocity along the lattice. Each node of the lattice acts as an automaton whose inputs are the neighboring nodes (Weisbuch, 1991). The final results are the statistical average of the lattice sites.

1.2.2 Different models

In this section, different lattice gas models are presented and described. Through these descriptions, a route of the evolution of these models can be traced and highlighted.

Usually, a lattice gas model consists of cells that form a triangular, hexagonal or square lattice and contained within each cell are the particles. To run a simulation process, one must:

- (1) Set up particles, cells, lattice, boundary conditions, and/or permeability. The particles have an initial velocity which is either uniform or obeys some distribution rules.
- (2) Allow particles to collide and propagate.
- (3) Obtain the particle configurations at the next step from current particle configurations.
- (4) Iterate step 2 and 3 in discrete time steps.
- (5) Average in space and in time in order to obtain a macroscopic description.

All the lattice gas models behave similarly according to the above five steps. Different models may adopt different rules to incorporate the above five procedures.

HPP Model

The HPP (Hardy, Pazzis and Pomeau, 1976) model uses a square lattice with insufficient symmetries to give the Navier-Stokes equations. Up to four duplicate particles lie in each cell. The particles have equal mass, equal speed, equal velocity and a direction coinciding with one of the four link directions. None of the identical particles will simultaneously occupy a vertex.

The simulation process includes two main steps: collision and propagation. The conservation of the number of particles and momentum holds through out the evolution. Since the particle's motion to a neighboring site is determined by its velocity at each time step, the rules of determining the next states of velocity remain unchanged except in the case when two particles have a head on collision.

The HPP model is not dynamically consistent, because the particles maintain a constant velocity. This model is a deterministic model in that the collision and propagation rules obey the conservation of mass, particle number and momentum.

The main disadvantage of the HPP model is that the lattice is not sufficiently symmetrical to model Navier-Stokes equations. The structure of the lattice determines the direction of the propagation of the particles. Frisch et al. (1986) proposed a triangular lattice or a hexagon lattice model which is the only 2D lattice able to maintain isotropy.

FHP model

In order to ensure isotropy, a triangular lattice is employed in the FHP model (Frisch, de Pazzis and Pomeau, 1986). The particles at the center of each cell can move along its six hexagonal neighboring cells. There may be several particles at a given site, but each velocity direction is subject to an exclusion principle of single occupancy.

Most of the set-up procedures of FHP model are similar to the HPP model except that in the FHP model, both binary and triple collisions are allowed. The updating of the lattice is done by alternating propagation and collision steps; the latter takes place at each individual site and the particles obey the same conservation laws as the true micro-scopic world, that is, conservation of the number and total momentum of the particles. This model can be regarded as a non-deterministic model because of the non-deterministic collision rule. The particles are discrete in space, time, and velocity. Therefore, no thermodynamics are involved in this model.

Multi-Speed model

The introduction of the multi-speed model (D’Humières, Lallemand and Frisch, 1986c; Chen et al., 1989) made it possible to conserve energy and introduce temperature. It uses a square 9-bit cellular automaton model. All particles have unit mass. The particles have discrete speeds of 0, 1, or $\sqrt{2}$, with the conventions that the particles moving along the axes have speed 1, the particles resting on the lattice have speed 0, while particles along diagonals have speed $\sqrt{2}$. At each time step, the particle number, energy and momentum are conserved, and there is at most one particle allowed in any applicable direction at each site; thus Fermi-Dirac statistics applies. The rule of propagation is that after colliding, the particles with speed 1 move to the nearest-neighboring sites, particles with speed $\sqrt{2}$ move to the next nearest-neighboring sites and particles with speed 0 stay.

The collision rules described by Chen et al. (1989) are quoted directly as follows:

- (1) In a head-on collision of two particles with speed 1, both particles leave the site along the directions perpendicular to their incident velocities with speed unchanged.
- (2) In a head-on collision of two particles with speed $\sqrt{2}$, both particles leave the site along the directions perpendicular to their incident velocities with speed unchanged.
- (3) In a collision between a speed $\sqrt{2}$ particle and a stopped particle, both particles change into speed 1 particles and leave at 45° with respect to the incident velocity. The inverse process is also allowed.
- (4) In a collision between speed 1 and speed $\sqrt{2}$ particle, the speed 1 particle reverses direction, and the speed $\sqrt{2}$ particle leaves along the other diagonal direction.

It should be noted from the above rules that the number of particles at a given speed is not conserved. However the total number of particles is conserved. Energy conservation is also independent of mass conservation.

FCHC model

D’Humières et al., (1986c) extended the 2-Dimensional (2D) FHP model to a 3-Dimensional (3D) Face-Centred-HyperCubic (FCHC) model by exploiting the existence of a four-dimensional lattice with all the required symmetries. For 3D simulation, the residing lattice is a three-dimensional projection of a FCHC model with unit periodicity in the fourth direction; it suffices to make the lattice one layer thick in the fourth dimension, giving it an effective 3D spatial structure. Isotropy is maintained in this model.

Thermodynamic automaton model

The principal characteristics of lattice gas models are that they are discrete in time, space and velocity, and the particles obey an exclusion principle because no more than one particle can occupy a particular velocity direction at any given site. Consequently, most models do not involve temperature. The other limitation of these models is that to achieve macroscopic isotropy, one must employ a triangular lattice in 2D and a four-dimensional face-centred hypercubic lattice in 3D simulations. Udey et al. (1999) constructed a new thermodynamic automata model that is different from the proceeding models. In this model, the momentum of a particle residing on a lattice is a continuous variable, allowing thermal effects to be captured. The particles are still discrete in time and space. However, probabilistic propagation rules and elastic binary scattering collision rules are applied, thus no restriction on lattice geometry exists. Lorentz invariant elastic collisions are used and the relativistic Boltzmann equation and the energy momentum tensor were rigorously derived from the collision and propagation rules using statistical mechanics. It is also easier to extend this 2D simulation to the 3D world.

1.2.3 Two approaches to Navier-Stokes equation

The Lattice Gas Automaton (LGA) has been used to simulate the Navier-Stokes equation for hydrodynamic systems for many automata models since its advent by Hardy de Pazzis and Pomeau(1976). Recently, an alternative method, the lattice Boltzmann automaton, based on the resolution of a Boltzmann equation, has been proposed as a new computational tool to investigate problems in the domain of fluid dynamics. (McNamara and Zanetti, 1988; Succi et al., 1991; Frisch, 1991; Holme, Richard and Rothman, 1992; Mora, 1992; Jiao, 1996). The application of lattice Boltzmann automata reduces some limitations of the lattice gas automata.

Lattice Gas Automata (LGA)

Lattice gas automata are based on the simulation of a very simple microscopic system, rather than on direct integration of partial differential equations (McNamara et al., 1988). Its dynamics is governed by local rules based on mass and momentum conservation. Particles hop between the sites of a regular lattice and may have collisions only on the lattice sites. The collision process is deterministic and is controlled by a set of collision rules.

Many authors (Frisch, 1991; Mcnamara and Zanetti, 1988; Balasubramanian et al., 1987) have tested the validity of the lattice gas scheme by simulating specific flow configurations that are analytic solutions to the Navier-Stokes equation. In all of these simulations, the state of the automaton is entirely specified in terms of a set of Boolean variables n_i which has the value 0 or 1 according to the motion of the particle. One can describe the microdynamical equations which govern the evolution of the Boolean field $n_i(x, t)$ (Succi et al., 1991).

$$T_i n_i \equiv n_i(x_j + c_i, t+1) - n_i(x_j, t) = \Omega_i(n) \quad (1.2)$$

Where $c_i (i=1, \dots, m)$ is the set of unit vectors connecting a given site of the lattice to its m neighbors; Ω_i represents the change in the i th occupation number due to the interaction of collision.; x_j is the position in j th cell, T_i is i th time step.

The collision term also obeys the following relations:

$$\sum_{i=1}^m \Omega_i = 0, \quad \sum_{i=1}^m \Omega_i c_i = 0 \quad (1.3)$$

Under the conditions of small Mach and Knudsen numbers (Frisch et al., 1987), starting from the above two equations, one can get the same structure as predicted by the Navier-Stokes equations.

The advantages of modelling physical systems using lattice gas automata as mentioned by Jiao (1996) are: bit efficiency; inherent simplicity; logical density and exact computability. In a lattice gas model, a single digital bit is used to represent a particle, thus avoiding the uncontrolled round-off errors in floating-point calculations. Consequently, it allows for high bit efficiency. Similar to statistical mechanics models, such as the Ising model, lattice gas automata are probably the simplest expression of Navier-Stokes flows. Compared to other numerical modelling of hydrodynamics, such as the finite difference or finite element method, lattice gas automata are easily implemented.

However, there are two main drawbacks to the lattice gas model. First, the microscopic dynamics of lattice gas automata are intrinsically noisy, requiring spatial and time averaging in order to study macroscopic properties. Second, lattice gas models are only valid when particles speed is small. If the Reynolds and Mach numbers are too large, the Navier-Stokes equation is no longer valid.

Lattice Boltzmann Automata (LBA)

The lattice Boltzmann approximation has been recently proposed as an alternative to Boolean lattice gas simulations (McNamara and Zanetti, 1988; Frisch, 1991). The idea is that one solves the lattice Boltzmann equation, which only aims to follow the evolution of the mean populations residing in the lattice instead of solving the Boolean equations which govern the microdynamic evolution of the cellular automaton. It is also noted that the lattice gas Boltzmann equation can be obtained from the full Boltzmann equation by an expansion procedure involving Hermite polynomials in the microscopic velocity (Grad, 1963).

The lattice Boltzmann equation is a nonlinear finite difference equation. Succi et al., (1991) presented the following difference equations obtained from the lattice Boltzmann equation.

$$T_i N_i = \sum_{j=1}^m \Omega_{ij} (N_j - N_j^{equil.}) \quad (1.4)$$

where $\Omega_{ij} = \frac{\partial \Omega_i}{\partial N_j}$ at $N_i = d$ which is given by

$$\Omega_{ij} = \sum_{ss'} (s'_i - s_i) d^{p-1} (1-d)^{m-p-1} A_{ss'} (s'_j - s_j) . \quad (1.5)$$

Here, d is the density per link of the discrete fluid; $A_{ss'}$ is the matrix element mediating the collision transforming the input state s into s' ; s and s' are Boolean strings of m bits; p is the number of particles involved in the collision, Ω_{ij} is the collision operator and $N_j^{equil.}$ is the equilibrium distribution expanded to the second order in the local velocity field.

A detailed derivation on how to obtain the Navier-Stokes equation from the lattice Boltzmann equation is given by Jiao (1996).

Compared to LGA, the advantage of the LBA is that it eliminates the large amount of noise which usually accompanies lattice gas automata. In addition, lattice gas automata are limited to low-speed regimes, while LBA are compatible with the aim of a large-scale description of the automaton fluid. Further, in contrast to the Fermi-Dirac equilibrium usually applied for the lattice gas method, the lattice Boltzmann automaton has more flexibility in the choice of the local equilibrium particle distribution.

However, there may still be differences between the incompressible Navier-Stokes equation and the macroscopic behavior of the discrete velocity Boltzmann equations because of the asymptotic nature of the Chapman-Enskog method. Since a real number (floating point) is used instead of a bit to represent the particle, the round-off error cannot be avoided.

1.3 Outline of the following chapters

The background of cellular automata, with a focus on its applications in hydrodynamic systems, has been reviewed in Chapter 1. A brief summary of the construction of a 2D thermodynamic automaton model based on Yang's model (1997) is presented in Chapter 2. Later in Chapter 3, a few simulations of fluid flow, including heat convection, turbulence, the Reynolds number, dispersion and diffusion in a tubes model and acoustic wave propagation in porous media are done using Yang's model. An attempt to extend the 2D thermodynamic automaton to 3D thermodynamic automaton model is described in Chapter 4. The 3D modelling of thermal equilibrium state is shown in Chapter 5, verifying the validity of the model. Further, in Chapter 5, more realistic simulations such as Darcy flow, Poiseuille flow, and diffusion in 3D spaces are implemented. Finally, conclusions of the present work and suggestions for further investigation are given in Chapter 6.

Chapter 2

Construction of a thermodynamic automaton model

Most traditional lattice gas models are based on the FHP model (Frisch et al., 1986). The limitation of the FHP model is its lack of temperature and the difficulty of maintaining symmetry in 3D domain. In order to incorporate temperature into an automaton model, Udey et al. (1997, 1999) constructed a relativistic thermal lattice gas model. A non-relativistic version of this model was later developed by Yang et al. (1997). A summary of the construction of this 2D thermodynamic automaton model (Yang, 1997) is presented in this chapter.

The model is formed according to the following principles:

- (1) Physical laws are introduced in the model, such as conservation of momentum, energy and particle types at the particle level.
- (2) The particles are allowed to populate a discrete space at a discrete time step.
- (3) Particles move freely through the lattice space by propagating probabilistically.
- (4) The boundary conditions can be set up to thermodynamic quantities, or conditions such as non-slip or slip boundaries can also be applied.
- (5) A porous medium may be introduced by setting a probability for a fluid-solid collision at each cell in space. Changing that probability will change the permeability or heterogeneity.
- (6) Multi-phase fluids are established by using different particle types.
- (7) Body and surface forces are introduced through the collision rules.

The detailed procedure for running a thermodynamic automaton simulation is as follows:

- (1) Set up cells and lattice (square lattice in this case) with different boundary conditions.
- (2) Choose a random number generator to generate a set of random number generators that are then assigned to each cell, thereby ensuring symmetric properties.

- (3) Assign a set of particles to each cell. The particle speed and direction is chosen which can be randomly set by the random generator or initialized to fit a Maxwell-Boltzmann distribution.
- (4) Randomly pick up pairs of particles. The selected pair will be removed and collide in the center of mass frame obeying a Lorentz invariant elastic collision rule or a non-relativistic elastic scattering rule. Then it will be transformed back to the center frame using the random deflection angle (0° to 360°).
- (5) The particles propagate according to probability rules defined in this section.
- (6) Iterate in time and repeat the collision and propagation cycles.
- (7) Output the results and obtain the macroscopic values by averaging procedures.

The Definition of probabilities (P) and the rules of propagation

There are four options for the motion of a particle: stay, move along the x -axes, move along the y -axes or move in the diagonal direction. Thus one can define four probabilities in equation 2.1.

$$\left. \begin{aligned} P_0 &= (1-V_a)(1-V_b) \\ P_a &= V_a(1-V_b) \\ P_b &= V_b(1-V_a) \\ P_{ab} &= V_a V_b \\ P_0 + P_a + P_b + P_{ab} &= 1 \end{aligned} \right\} , \quad (2.1)$$

where $V_a < 1$, $V_b < 1$.

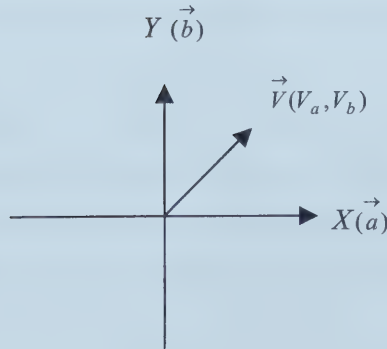


Figure 2.1 Diagram of XY coordinates for the motion of the particles.

where, a and b represent the two principal directions which correspond to the x and y axes for a square lattice (Figure 2.1).

A random probability (p) is produced. Particles will propagate according to the relationship between generated and calculated probabilities:

- (1) If $p < P_0$, the particle stays;
- (2) If $P_0 < p < P_0 + P_a$, the particle move along a ;
- (3) If $P_0 + P_a < p < P_0 + P_a + P_b$, the particle moves along b ;
- (4) If $P_0 + P_a + P_b < p$, the particle move along ab .

The main properties and the consequences of the thermodynamic model are:

- (1) Because of the probabilistic collision rules, the lattice simply acts as a book keeper.
Thus the model is compatible with any lattice geometry without losing isotropy.
- (2) There is no limitation on the number of particles assigned in each cell, and no exclusion principle is applied, which provides a better representation of the statistics.
However, the larger number of particles, the more computational time.
- (3) Thermal effects are captured due to continuous particle momentum.
- (4) It is straightforward to extend to 3D models while maintaining the isotropy.
- (5) Probabilistic rules are applied instead of deterministic collision and propagation rules.
Only binary elastic collisions are considered because triple binary collisions are rare and should not significantly affect the results.
- (6) The speed of particles is within the range of zero and one with one value corresponding to the speed of light in the relativistic model. In the non-relativistic model the velocity is dimensionless. For an average velocity less than 0.2, the probability of a particle traveling faster than one is so rare that such particles may be ignored.

Chapter 3

Applications of 2D thermodynamic automata

3.1 Introduction

Chapter 2 presented detailed rules about constructing a 2D thermodynamic automaton model. This model has been applied to diffusion and dispersion problems by Yang (1997). This chapter will apply it to other aspects of fluid flow. First, particle number distribution due to gravity is modelled and then is followed by a simulation of laminar and turbulent flow, in which the Reynolds number is calculated. Later, heat convection is modelled, which clearly indicates that temperature is the internal property of a 2D thermodynamic automaton model. Diffusion and dispersion in porous media is also simulated by varying the tubes widths. Finally, acoustic wave propagation in a porous medium is modeled.

3.2 Modelling particle number distribution

In this section, a thermodynamic automaton model with four thermodynamic boundaries is used to obtain the distribution of particles number due to gravity. The results are in agreement with the analytic solution.

3.2.1 Theoretical background

In statistical physics, if the motion of gas molecules is governed by classical mechanics, one could introduce a molecule distribution in phase space in place of the distribution over quantum states (Landau and Lifshitz, 1958). Consider a gas which is in an external field in which the potential energy of a molecule is a function of the co-ordinates of its center of gravity alone: $U=U(x, y, z)$. If the translational motion in this field is quasi-classical (as it always is in practice), then $U(x, y, z)$ enters into the energy of the molecule as an independent additive quantity. The Maxwell distribution over the coordinates of the center of gravity is given by the formula

$$dN_r = n_0 e^{-u(x,y,z)/KT} dv, \quad (3.1)$$

where dN_r is the average number of molecules enclosed in the volume element of phase space for a molecule. v is the volume. T is temperature. K is a constant.

This equation shows the number of molecules in the volume element $dV=dx dy dz$; the term

$$n(r) = n_0 e^{-u(x,y,z)/KT}, \quad (3.2)$$

represents the density of the particles. Formula (3.2) is the Boltzmann formula.

In a uniform gravitational field directed along the z axis, $u(x, y, z)=mgz$, where m is the mass of a molecule, g is gravity acceleration. The density distribution of the gas is then given by what is called Barometric formula

$$n(z)=n_0 e^{-mgz/KT} \quad (3.3)$$

where n_0 is the density at the level $z = 0$.

3.2.2 Model and simulation results

The model to simulate the above barometric formula has been constructed as follows:

- (1) The lattice size is 100×10 (100 unit length in x direction), with an initialization of the particles all having the same mass, and the speed obeying Maxwell-Boltzmann distribution.
- (2) Each cell has 10 particles, so that the total number of particles was 10000.
- (3) Four thermodynamic boundaries with the same $\beta=200$, corresponding to average velocity $v=0.1$ were assigned.
- (4) In each time step, a pump with the momentum of 0.001 is added horizontally to each particles acting as a gravity force.

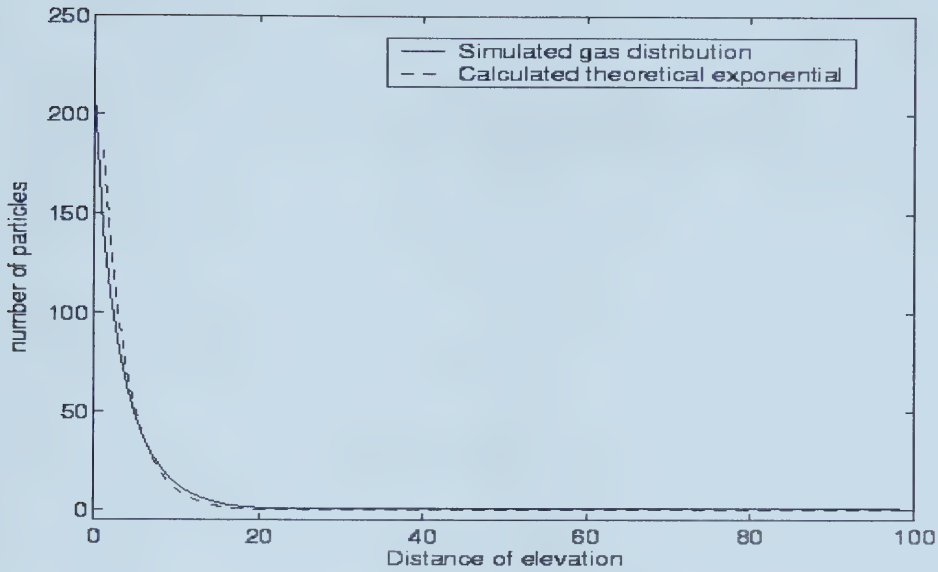


Figure 3.1 2D simulation of gas distribution due to gravity by averaging the rows (solid line) and calculated theoretical distribution (dash line)

The simulations was run for 5000 time iterations, the results are shown in the following figures.

Figure 3.1 shows the average gas distribution for each column. The simulation results are in good agreement with the analytical calculation. In order to get close view of the simulation at different steps, Figure 3.2 plots the natural logarithm of gas number at three different time steps : 1000, 2000 and 5000. It is expected to get three straight lines according to logarithm of equation 3.3. However, due to insufficient particle number, the gas number at higher elevation is around zero, so the line is not straight. Figure 3.2 also shows that the longer the simulation the straighter the line. It suggests that when the simulation goes longer, the simulation converges which is also verified by Figure 3.3. Figure 3.3 shows that the simulation results from 4000 time steps and 5000 time steps are almost the same which suggests that the longer iteration makes no difference any more once the simulation results converged.

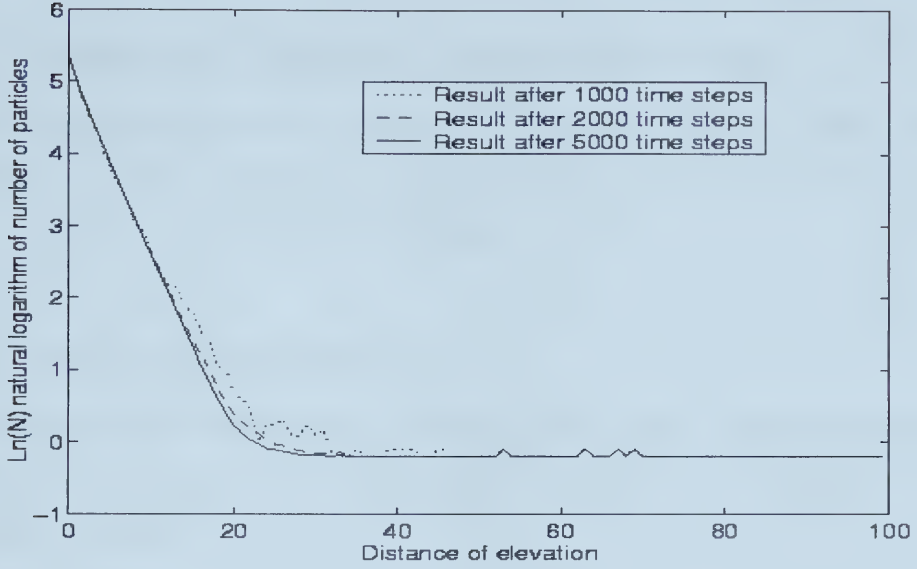


Figure 3.2 Plot of natural logarithm of Gas number distribution due to gravity versus elevation at different time steps.

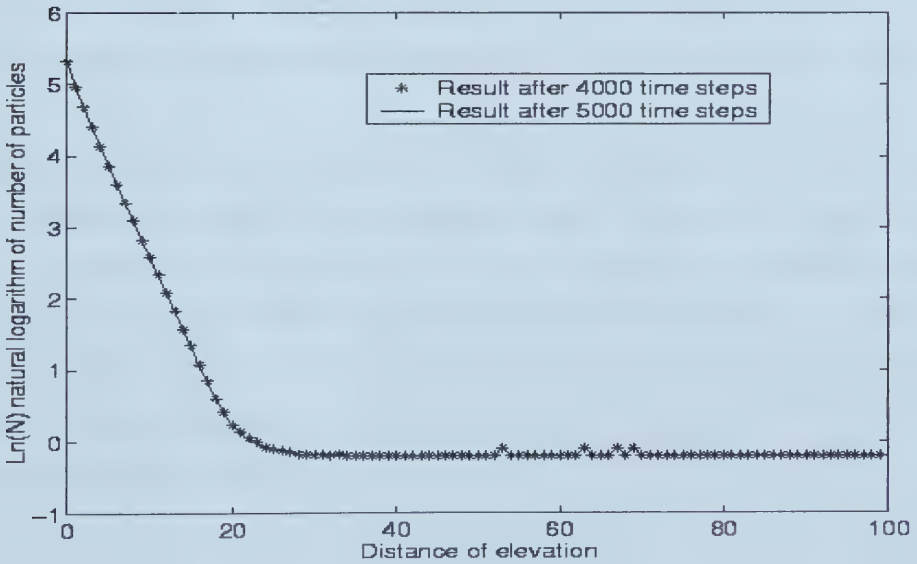


Figure 3.3 Plot of natural logarithm of Gas number distribution due to gravity versus elevation at time steps 4000 and 5000.

3.3 Laminar flow, Turbulence and Reynolds number

In this section, a background to laminar flow and turbulence is given. A thermodynamic automaton model is modified to simulate laminar and turbulent flow and the corresponding Reynolds numbers are calculated.

3.3.1 Theoretical background

When a fluid (gas or liquid) flows between two plates or in a pipe, the flow rate (the volume of fluid flowing per unit time) through the pipe can be described by Poiseuille's equation (Zemansky, 1957).

$$V = \frac{\pi D^4}{128 \eta} \frac{P_1 - P_2}{L} \quad (3.4)$$

where D is the diameter of the pipe; p_1 and p_2 are the pressure of two sides; L is the length of the pipe, η is viscosity of the fluid, and V is volume flow rate of the fluid.

Experimental work has shown that four factors determine whether the fluid flow through a pipe is laminar or turbulent. This combination is now known as the Reynolds number (R). The experimental data also indicates that when R increases, it eventually reaches a value R_{cr} (the critical Reynolds number) beyond which the flow is unstable and turbulence arises. Landau and Lifshitz (1959) stated that although the critical Reynolds number is not, of course, a universal constant, these values appear to be of order of 10 to 100. Reynolds number is defined as:

$$R = \frac{\rho V L}{\eta} \quad (3.5)$$

Where ρ is the density, V is average flow velocity, l is the length of the tube, η is fluid viscosity, R is Reynolds number. It is easily seen that Reynolds number is dimensionless, since it is unitless.

The following figure shows velocity vectors in laminar flow and turbulent flow.

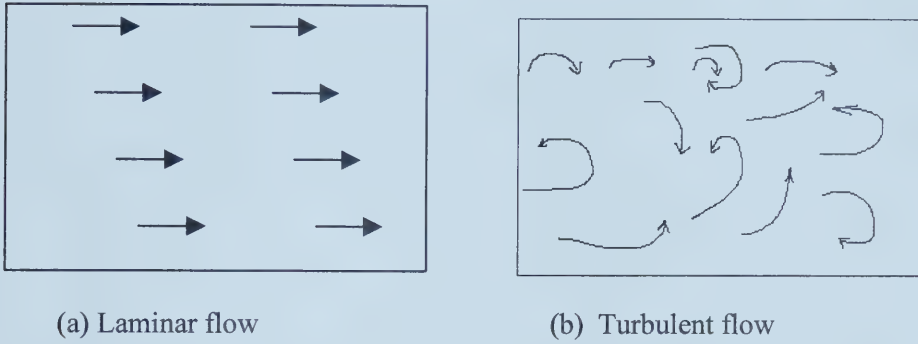


Figure 3.4 Diagram of the velocity vectors for laminar flow (a), and turbulent flow (b)

3.3.2 Models and numerical simulations

First, the lattice to investigate the laminar and turbulent flow was constructed. The lattice size was 100×10 , the other variables such as velocity, boundary temperature, are the same as in section 3.2 except that the left and right boundaries were designed as a periodic boundary and a pressure drop was added from left to right. Two different pressure drops were tested, $p=0.00001$ and $p=0.0001$. Here, velocity profiles in both directions and energy profiles of the two cases are presented. This shows the change from laminar flow to turbulence.

The similar shape of horizontal velocity profiles in Figure 3.5 and Figure 3.6 indicates that the velocity in horizontal direction is not affected when flow changes from laminar flow to the onset of turbulence. Also, the velocity in the middle of the pipe is greater than in the rest of the pipe. In Figure 3.7, the vertical velocities of laminar flow are almost the same, which means the velocity vectors for laminar flow are parallel vectors. While in

Figure 3.8, the vertical velocities vary largely on each position. The onset of turbulence is tested by increasing the pressure drop gradually from 0.00001 to 0.005. Only when the pressure drop is 0.0001 can a large vertical velocity difference be observed between each position. Therefore, it is likely that turbulence starts when pressure drop equals 0.0001. This is verified by the velocity vectors in Figure 3.9(a) to 3.9(e). For turbulent flow, the velocity vectors no longer point in the same direction as they do in laminar flow.

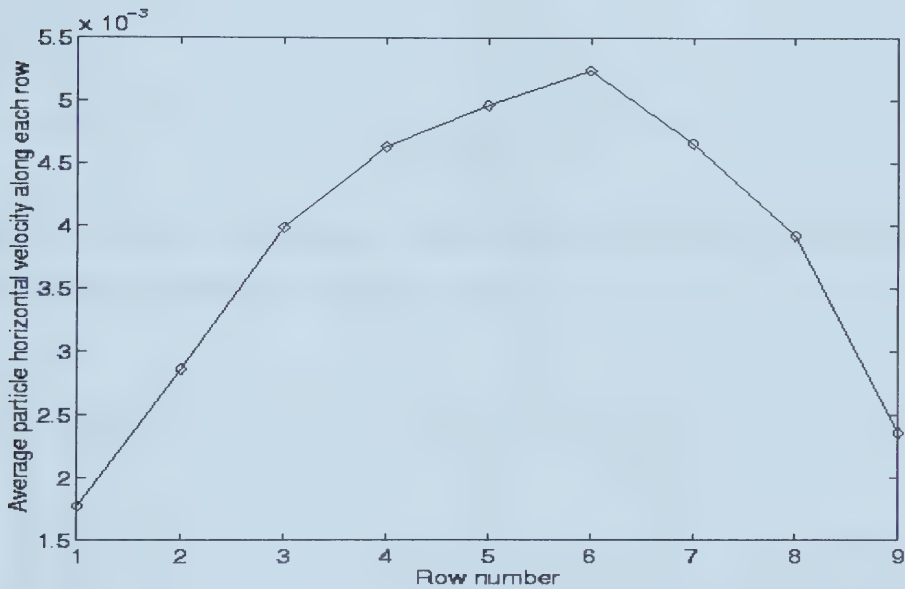


Figure 3.5 Particle velocity in the x-axis direction, determined by averaging along each row for laminar flow (pressure drop=0.00001).

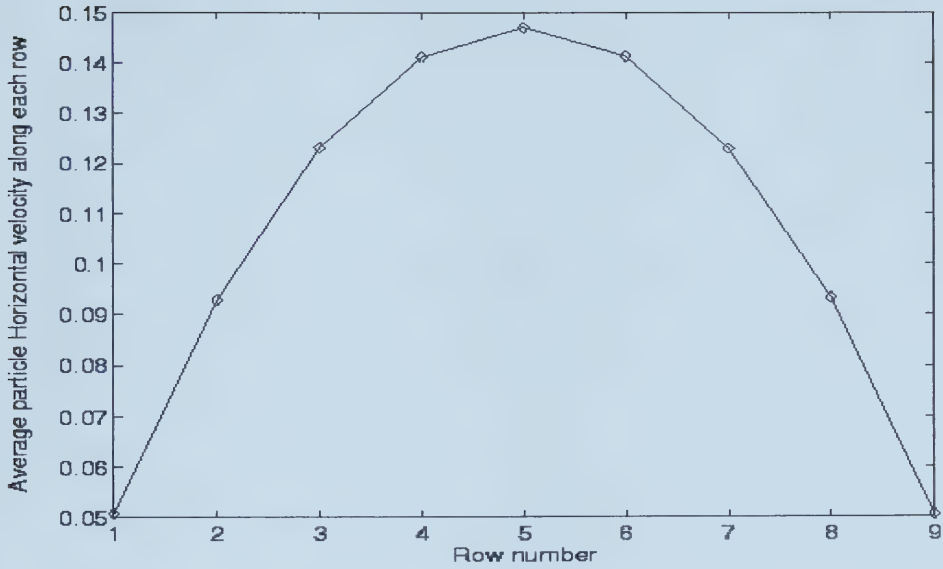


Figure 3.6 Particle velocity in the x -axis direction, determined by averaging along each row for turbulence (pressure drop=0.0001).

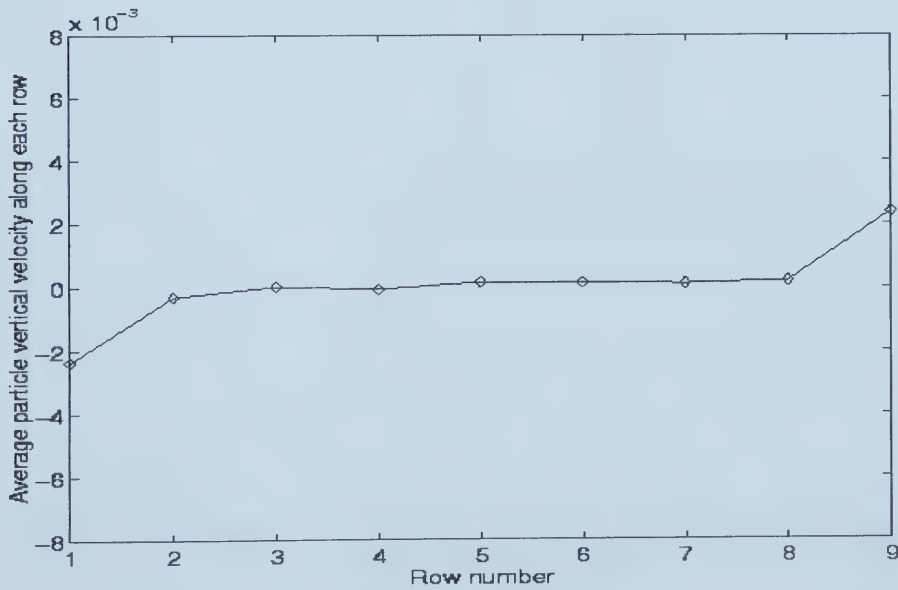


Figure 3.7 Particle velocity in y -axis direction, determined by averaging along each row for laminar flow (pressure drop = 0.00001).

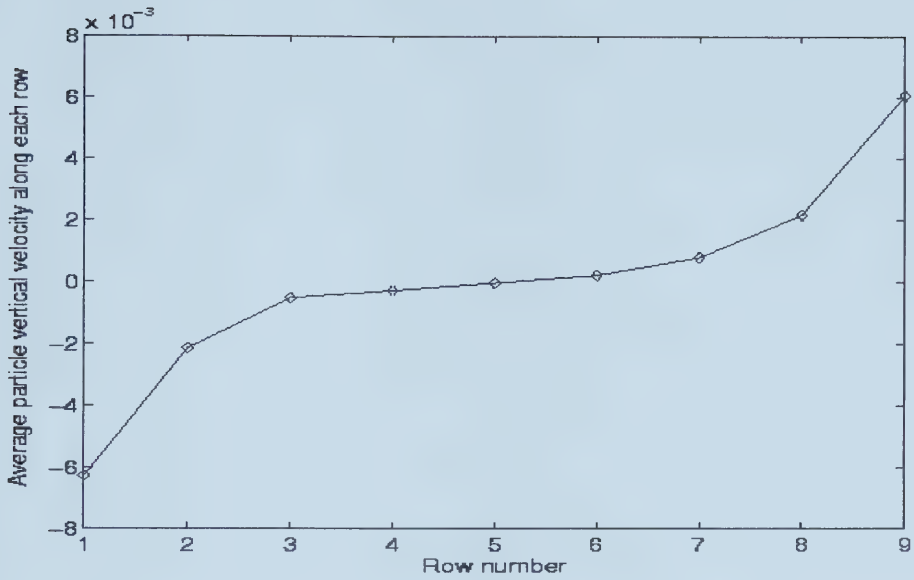


Figure 3.8 Particle velocity in y -axis direction, determined by averaging along each row for turbulence (pressure drop=0.0001).

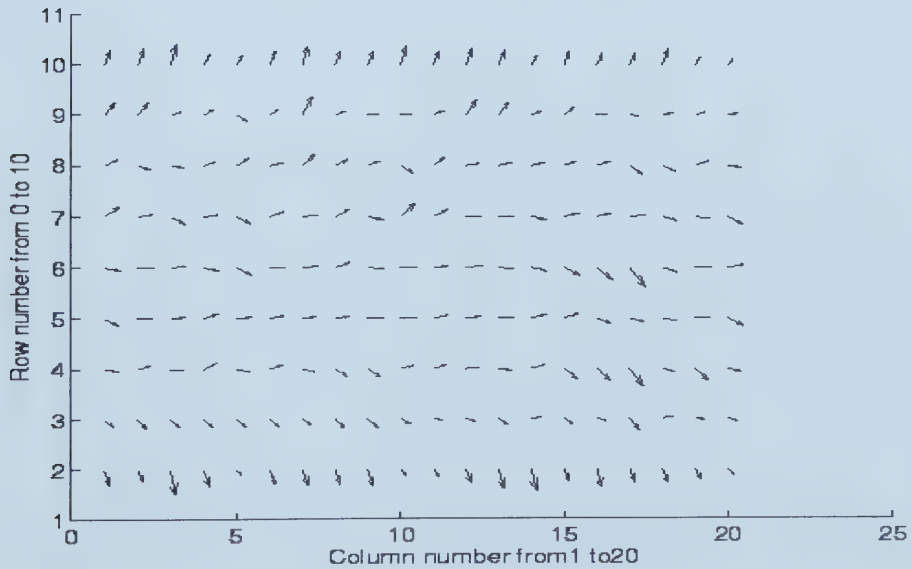


Figure 3.9 (a) Particle Velocity vectors for the onset of turbulence, columns 1 to 20, the pressure drop (0.0001) has been added along horizontal direction.

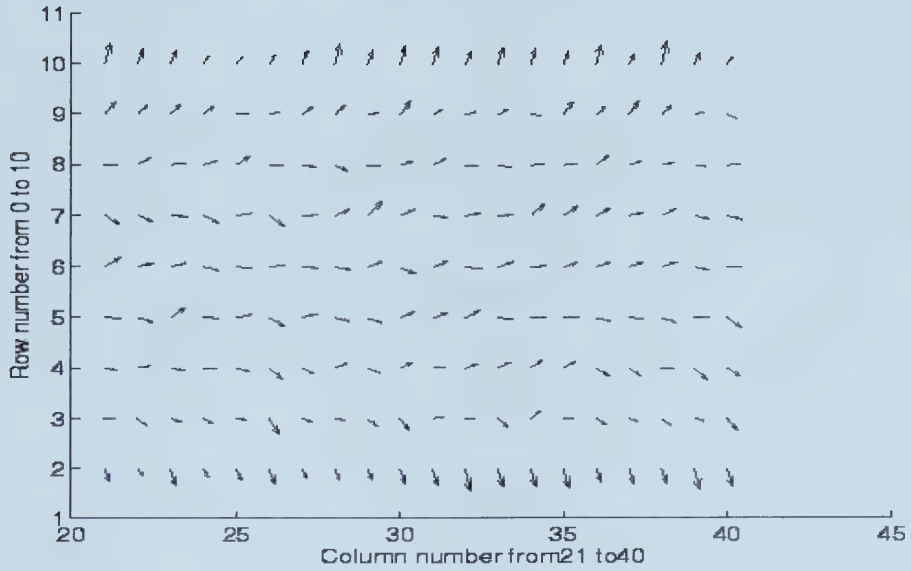


Figure 3.9 (b) Particle Velocity vectors for the onset of turbulence, columns 21 to 40, the pressure drop (0.0001) has been added along horizontal direction.

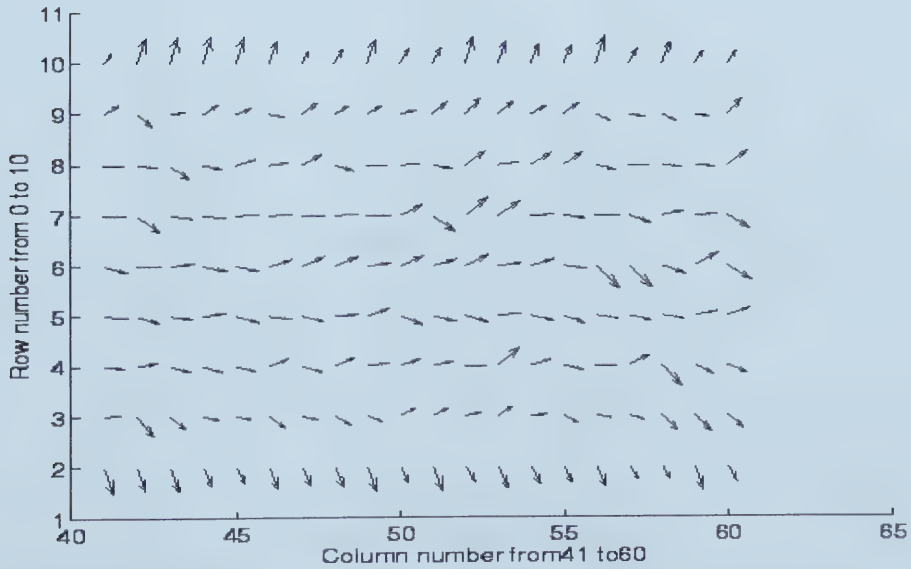


Figure 3.9 (c) Particle Velocity vectors for the onset of turbulence, columns 41 to 60, the pressure drop (0.0001) has been added along horizontal direction.

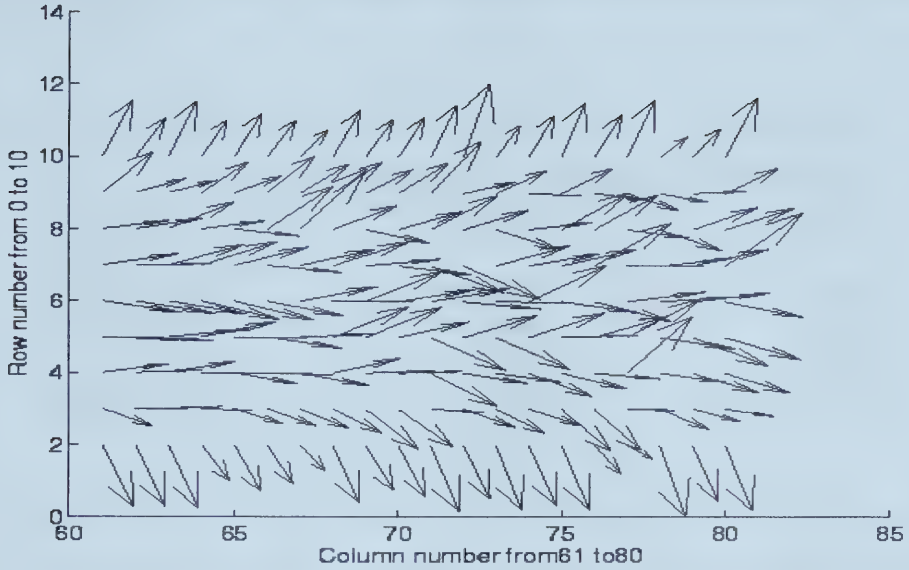


Figure 3.9 (d) Particle Velocity vectors for the onset of turbulence, columns 61 to 80, the pressure drop (0.0001) has been added along horizontal direction.

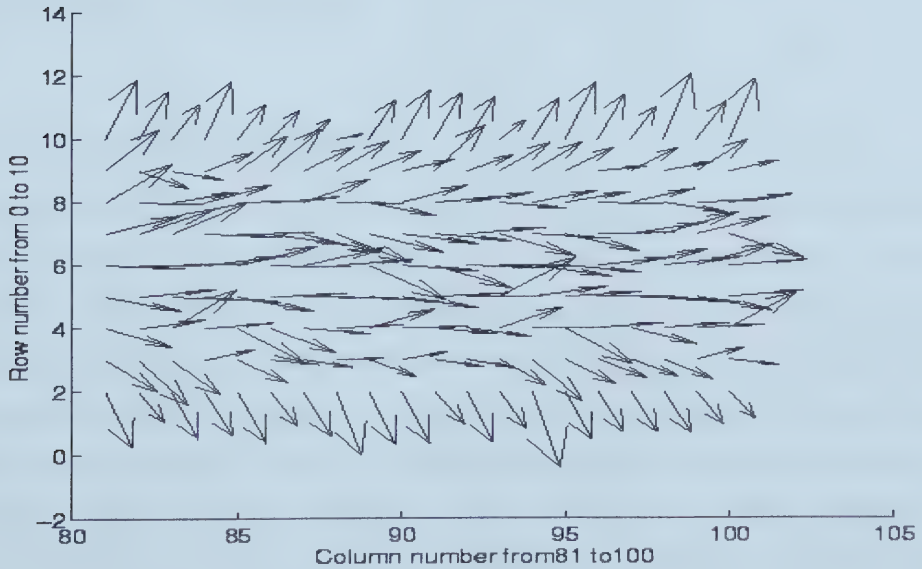


Figure 3.9 (e) Particle Velocity vectors for the onset of turbulence, columns 81 to 100, the pressure drop (0.0001) has been added along horizontal direction.

The Reynolds number for both models is calculated according to equation 3.5. The data are listed in table 1.

Table 1 Reynolds number of laminar flow and the onset of turbulent flow

	Laminar flow	the onset of turbulent flow
Average flow velocity	0.0038	0.0286
Radius of the pipe	5	5
Pressure drop	0.00001	0.0001
Fluid viscosity	0.0222	0.0291
Particles density	10.0001	10.0002
Reynolds number	8.45	49.16

The calculated critical Reynolds number (49.16) is within the range 10 to 100 mentioned above. One can conclude that the simulation results are consistent with the experiment results.

3.4 Heat convection

In this section, heat convection is modelled by heating a sealed box from one boundary, and then observing the velocity field.

3.4.1 Theoretical background

A current of liquid or gas that absorbs heat at one place and then moves to another place, where it mixes with a cooler portion of the fluid and rejects heat, is called heat convection (Zemansky, 1957). The temperature distribution in a fluid at very high Reynolds numbers is similar to that of the velocity distribution. In the turbulent region, a considerable exchange of heat occurs, which is due to the intensive mixing that takes place in a turbulent flow. Thus, the process of heat transfer in laminar and turbulent flow is fundamentally different (Zemansky, 1957). Here, one mainly discusses free convection. If heat convection happens, the mechanical equilibrium of convection breaks.

A special case of convection simulated here is the flow that occurs in a box of fluid, where the vertical planes have different temperatures. The lower plane (T_2) is greater than

that of upper plane (T_l). If the temperature difference $T_2 - T_l$ is small, the fluid remains at rest and there is pure thermal conduction. However if the difference $T_2 - T_l$ exceeds a critical value, which depends on the distance between the plates, such a state becomes unstable and steady convection occurs. For very large temperature differences, the steady convection turn becomes turbulent (Landau and Lifshitz, 1959).

3.4.2 Models and numerical simulations

The model for heat convection is the same as the model for particle distribution due to gravity, except that there is no pressure in this model. The left, top, and bottom boundaries are thermodynamically defined with the same temperature as the internal particles. The right boundary is supplied with a temperature 200 times higher than that of the other boundaries. The simulation results are presented in Figure 3.10 to Figure 3.15.

Figure 3.10, Figure 3.12, and Figure 3.14 are the particle velocity vectors before heating. The disorder of the vectors indicates equilibrium state. Note that in Figure 3.15, the velocity vectors point in the direction opposite to the heated boundary. Also note that for positions far away from the heating source, the heat convection is small (Figure 3.11, Figure 3.13). Closer to the heating source, the heat convection is more obvious. One can conclude that the heat convection simulation is consistent with theoretical expectations.

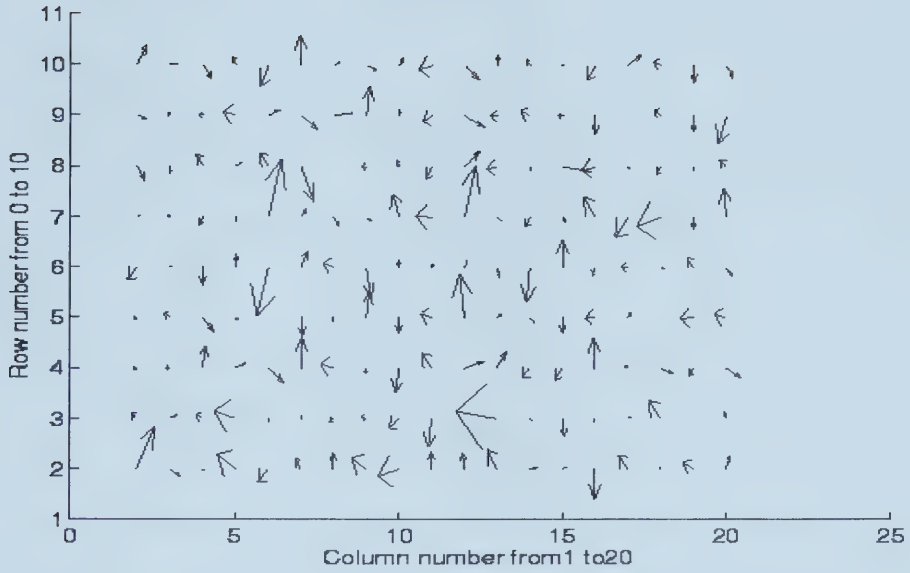


Figure 3.10 Particle velocity vectors at an equilibrium state before heating, columns 1 to 20.

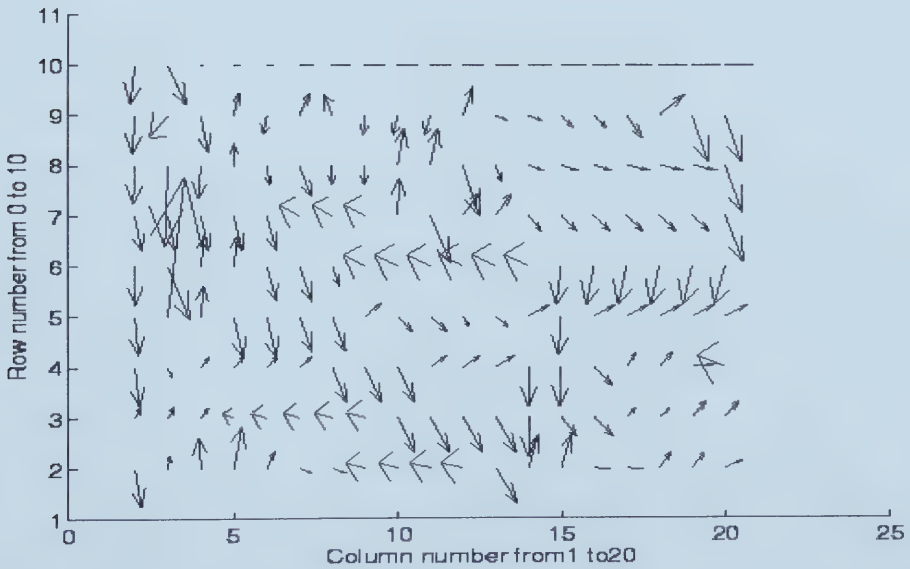


Figure 3.11 Particle velocity vectors at an equilibrium state after heating, columns 1 to 20 after 5000 time steps

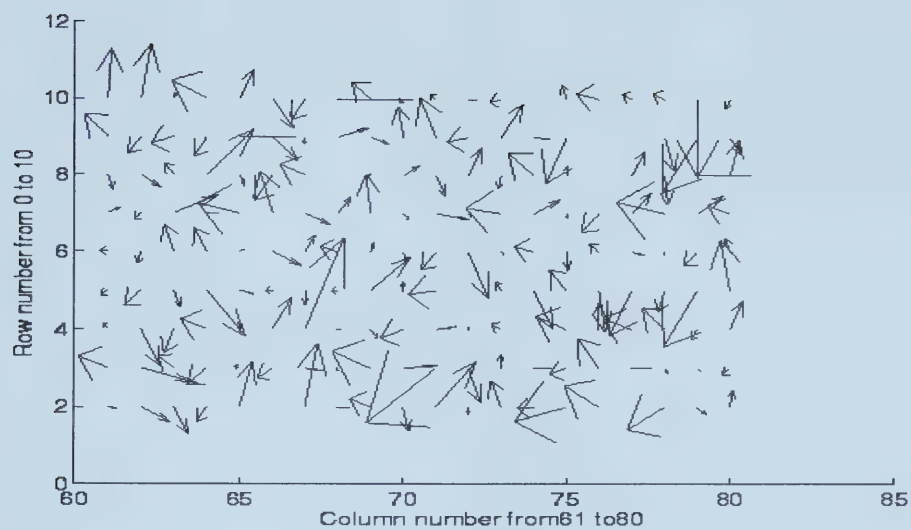


Figure 3.12 Particle velocity vectors at an equilibrium state before heating, columns 61 to 80

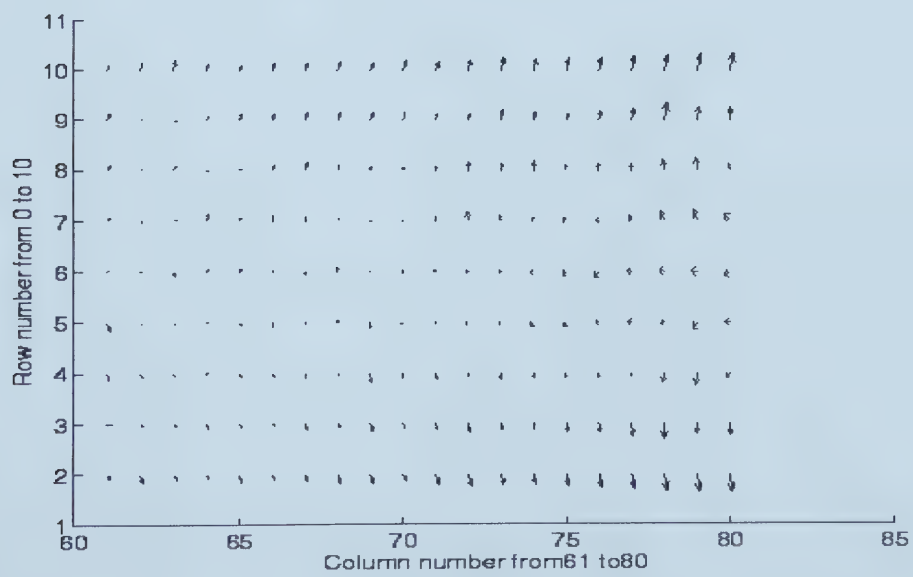


Figure 3.13 Particle velocity vectors at an equilibrium state after heating, columns 61 to 80 after 5000 time steps

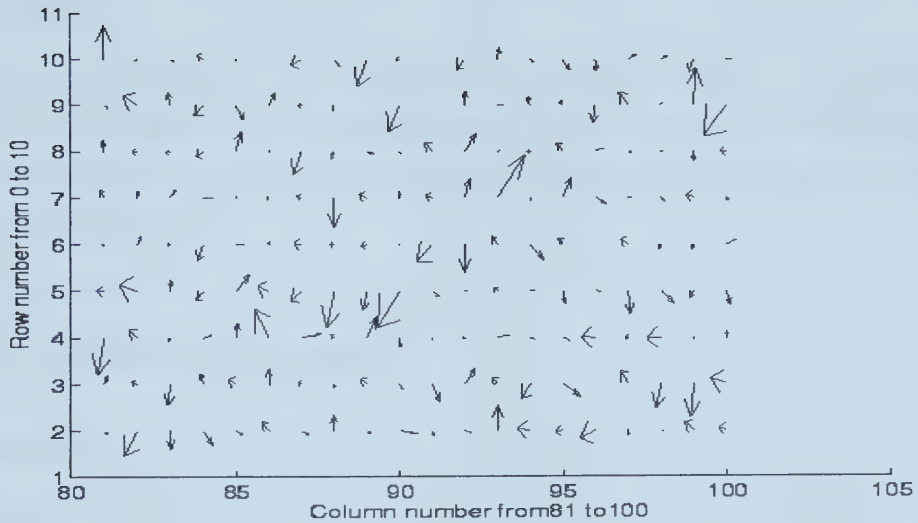


Figure 3.14 Particle velocity vectors at an equilibrium state before heating, columns 81 to 100

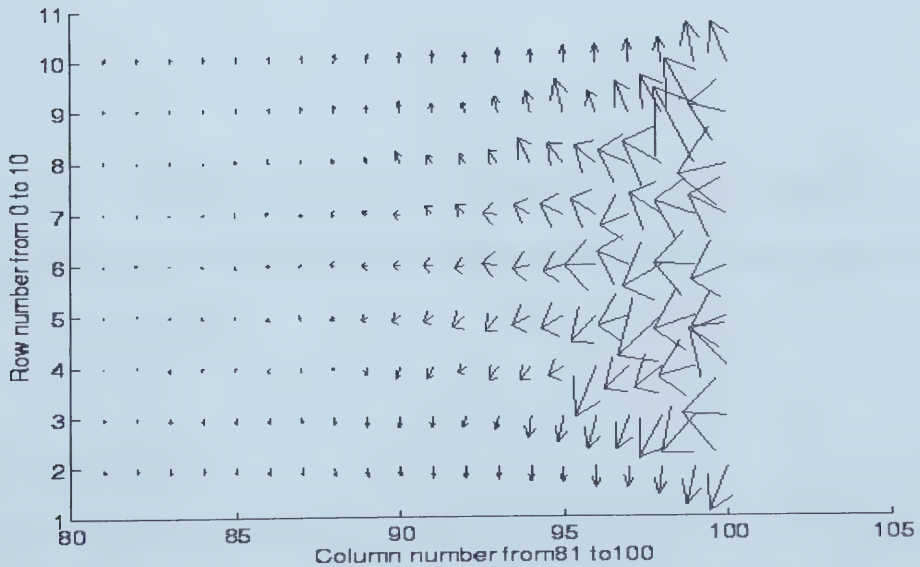


Figure 3.15 Particle velocity vectors at an equilibrium state after heating, columns 81 to 100 after 5000 time steps

3.5 Diffusion and dispersion in porous media using the tubes model

In this section, fluid flow in both homogeneous and heterogeneous porous media is studied with a focus on diffusion and dispersion. The permeability has been incorporated by introducing a set of tubes to the model. Heterogeneity has been obtained by varying the width of each tube.

3.5.1 Theoretical background

Darcy flow

An experiment done by Darcy (1856) showed that the volumetric flow rate of fluid through a porous medium is directly proportional to the applied pressure drop and is inversely proportional to the fluid viscosity. This empirical relationship is the so-called Darcy's law, which has been theoretically derived by a number of researchers (Newman, 1977; Whitaker, 1986). In one dimension, Darcy's law is given by the simple equation

$$q = -\frac{K}{\mu} \frac{dp}{dx}, \quad (3.6)$$

where q is the volumetric flow rate, K is permeability of the porous medium, which is a fundamental property of the geometry of a porous medium, $\frac{dp}{dx}$ is the applied pressure drop, μ is fluid viscosity.

Two-phase flow

The equations of motion for steady two-phase fluid flow are given by de la Cruz and Spanos (1983).

$$Q_{11}q_1 - Q_{12}q_2 = -\frac{\partial p_1}{\partial x} \quad (3.7)$$

$$Q_{22}q_2 - Q_{21}q_1 = -\frac{\partial p_2}{\partial x} \quad (3.8)$$

$$\frac{\partial p_c}{\partial t} = \beta_1 \frac{\partial s_1}{\partial t} + \beta_2 \frac{\partial^2 s_1}{\partial t^2} \quad (3.9)$$

where Q is the mobility ratio, q is the flow rate, $\frac{\partial p}{\partial x}$ is the pressure gradient, ρ is the density of a fluid, s is the saturation, and subscripts 1 and 2 refer to phase 1 and 2, respectively. β is a constant.

Diffusion equation

Diffusion occurs from high to low concentration areas due to molecular motion (Yang, 1997). For a fluid diffusing in a tube, the diffusion equation is

$$\frac{\partial c}{\partial t} = D \frac{\partial^2 c}{\partial x^2} \quad (3.10)$$

where c is tracer concentration and D is the diffusion coefficient. When diffusion occurs in a porous medium, the apparent diffusion coefficient (D_a) is used in equation 3.10, which is less than the molecular coefficient D as measured in a tube. Solutions of the above equation are related to the symmetric Gauss function.

Dispersion equation

Dispersion has been referred to as the spreading of a tracer released into a flowing fluid (Baudet, 1989). Dispersion includes two important mechanisms: diffusion and convection. Therefore, dispersion of miscible flow for a two-phase fluid in porous media is traditionally described by the convection-diffusion equation (Fried, 1971)

$$\frac{\partial c}{\partial t} + v_x \frac{\partial c}{\partial x} = D_l \frac{\partial^2 c}{\partial x^2} \quad (3.11)$$

Here v_x is the mean volumetric velocity in the x direction; D_l is the longitudinal dispersion coefficient and t is the time. Solutions for this equation are available for various initial and boundary conditions (Bear, 1972). Usually the solution of this equation is related to the Gauss-error function.

However, equation 3.11 can not completely describe the nature of two-phase miscible fluid dispersion because during the dispersion process, the pressure drop and saturation changes from point to point. And if one phase is displacing another, a pressure gradient must exist between the displacing and displaced phases. Therefore, the revised dispersion equation of miscible flow with negligible molecular diffusion and an extra pressure equation are used here (Udey and Spanos, 1993).

$$\left. \begin{aligned} \frac{\partial c_{f2}}{\partial t} + v \cdot \nabla c_{f2} &= \frac{1}{\rho} \nabla \cdot (\rho D_m \cdot \nabla c_{f2}) \\ p_1 - p_2 &= \beta \frac{\partial c}{\partial t} \end{aligned} \right\} \quad (3.12)$$

where c_{f2} is fractional mass concentration of fluid 2, v is the macro scale velocity of momentum flux, ρ is macro scale fluid density and D_m is the apparent mechanical tensor, t is the time, p_1 is the pressure in the fluid 1 and p_2 is the pressure in the fluid 2, β is a constant.

It is important to note that, unlike the dispersion tensor D_l in equation 3.11, this apparent dispersion tensor D_m is not a constant. It varies in value from point to point in the flow. Actually, it depends upon the concentration, the concentration gradient, and the flow rate.

In this paper, tubes with different widths were used to model the porous medium for both homogeneous and heterogeneous cases. The principle of changing tube width in order to change the porosity is as follows:

According to the detailed version of Darcy's law (Simplified Navier-Stokes equation)

$$\mu \frac{d^2 u}{dz^2} = \frac{\partial p}{\partial x} \quad (3.13)$$

Integrating the above equation in the z direction and applying boundary condition $u=0$ for $z=0$ and $z=h$, one gets

$$\Phi = \frac{\int_0^h u dz}{h} = \left(\frac{h^2}{12} \right) \frac{p}{\mu} \quad (3.14)$$

where u is fluid velocity; x, z represent two directions, μ is viscosity, h is the tube width, p is pressure, Φ is velocity potential.

Comparing equation 3.14 with equation 3.6, one can see the permeability k in equation 3.6, is similar to the term $\frac{h^2}{12}$ in equation 3.14. Thus, increasing the tube width will increase the permeability.

3.5.2 Models and simulation results

The tube models used are listed in Figure 3.16. For both diffusion and dispersion experiments in homogeneous and heterogeneous media, an initial configuration is constructed with a random initialization of 20 particles with a thermal equilibrium state at a temperature of 0.005 (mass being 1.0, velocity being 0.1) in each cell. A thermodynamic boundary condition is applied to top and bottom boundaries and a periodic boundary condition is assigned to left and right boundaries. The lattice size is 500×100 ; the tracing particles are assigned in the middle of the tube according to the x

direction. For diffusion, the pressure is zero, and for dispersion two pressure gradients are tried $p=0.0025$ and $p=0.001$.

As in Figure 3.16, for a homogeneous medium, ten tubes with the same width of 10 are used, and in the heterogeneous media ten tubes with different size are used while the permeabilities of both models are kept the same. In the heterogeneous case, the permeability in each tube varies with tube width.

Figure 3.17 ~ 3.21 show diffusion in homogeneous and heterogeneous media. From the average of all tubes or the average of a specific tube or from a comparison of diffusion in both media, it is clear that there is not much difference among all the cases, which means diffusion is not affected to a significant degree by the structure of medium so long as the permeability is the same. As well the figures all show that diffusion process happens slowly.

Figure 3.22 shows that larger the pressure, faster the dispersion. Figure 3.23 shows that dispersion happens with the time. It evolves from a symmetric diffusion curve (step=100) to asymmetric dispersion curve (step=400). Figure 3.24 differs from Figure 3.23, in that there are two peaks. This suggests fluid is separating due to the width of the tubes. In Figure 3.25, the dispersion process in homogeneous and in heterogeneous media are compared. One can observe that dispersion is much faster in the heterogeneous medium. Figure 3.26 shows that dispersion in each tube in the homogeneous media is the same, while in Figure 3.27, dispersion speed in the big tube is faster than in the small tube. Here, one can conclude that the different speeds in specific tubes cause the two peaks in Figure 3.24.

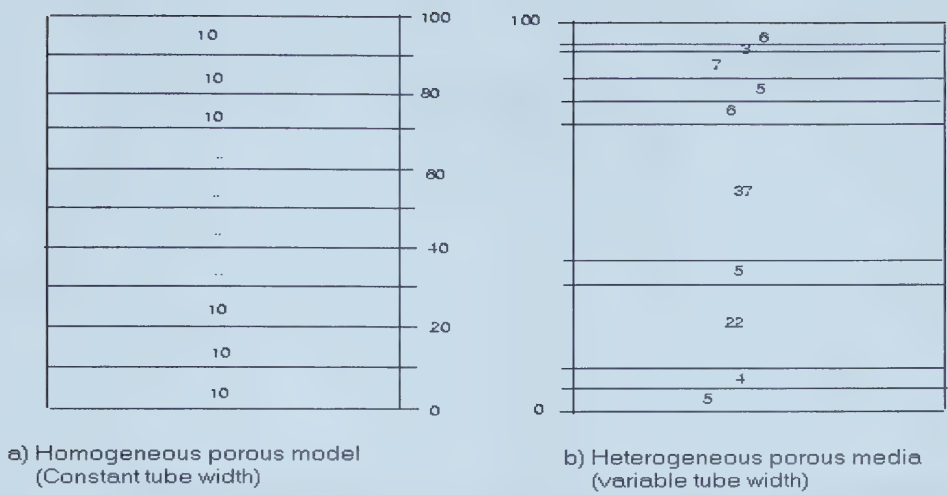


Figure 3.16 Schematic diagrams of tube models

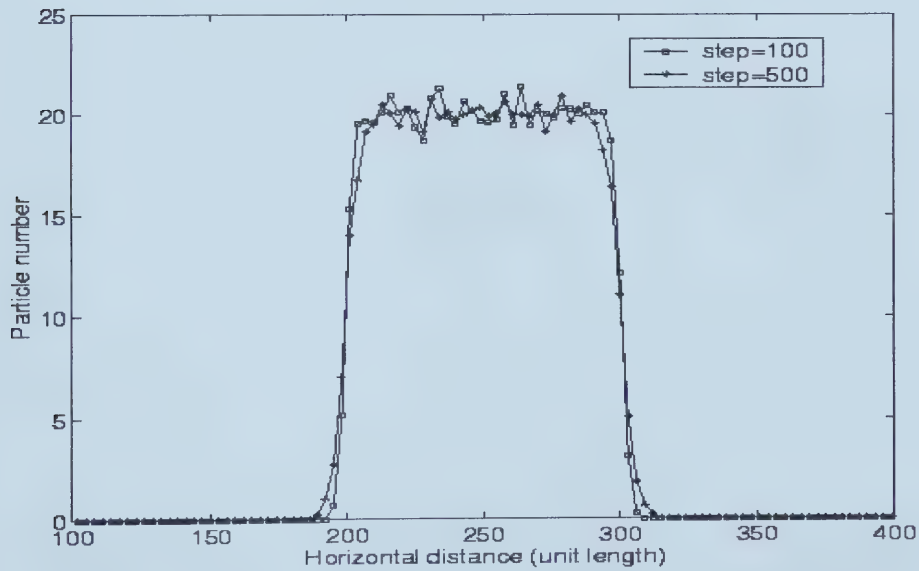


Figure 3.17 Diffusion in a homogeneous porous medium (average of all tubes), using the model in Figure 3.16 (a).

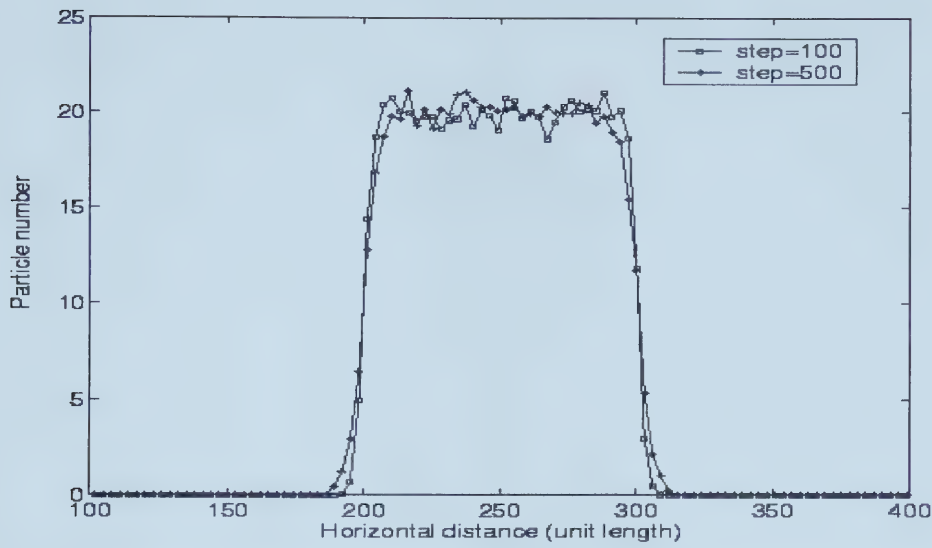


Figure 3.18 Diffusion in a heterogeneous porous medium (average of all tubes), using the model in Figure 3.16 (b).

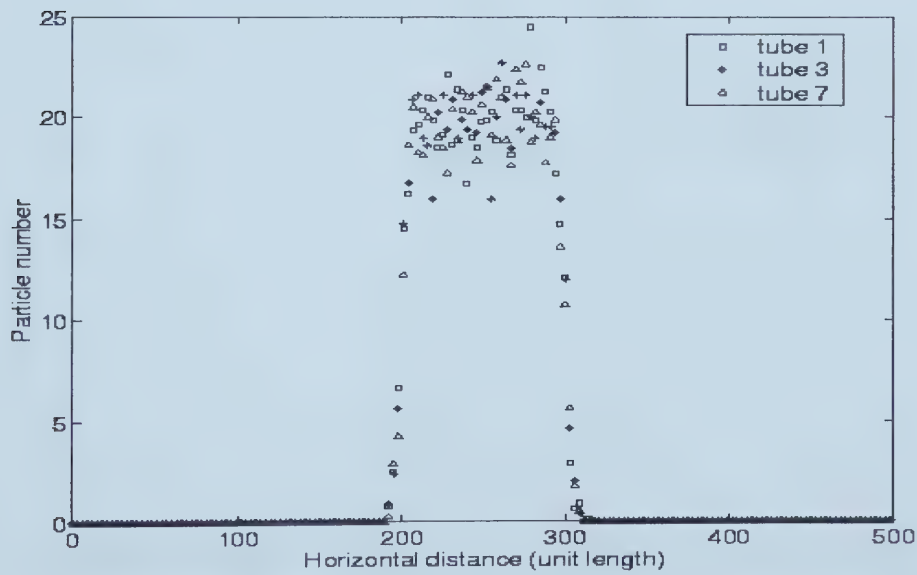


Figure 3.19 Diffusion in a homogeneous porous medium (specific tube averages), using the model in Figure 3.16 (a), after 300 iterations.

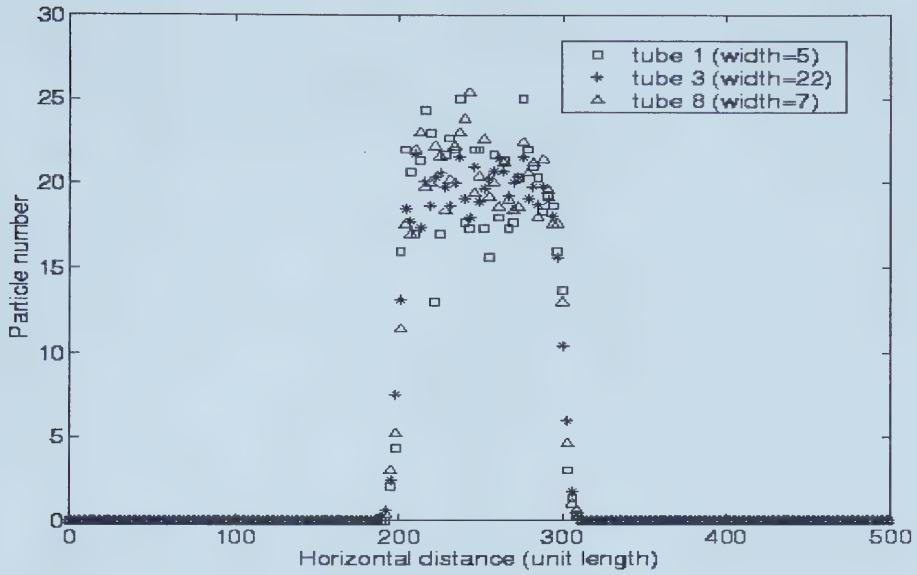


Figure 3.20 Diffusion in a heterogeneous porous medium (specific tube averages), using the model in Figure 3.16 (b), after 300 iterations.

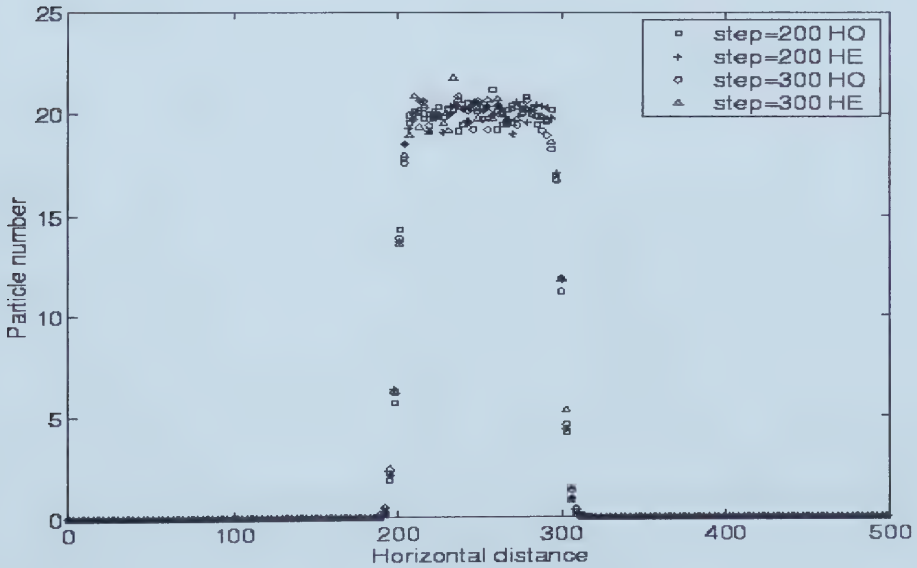


Figure 3.21 Comparison of diffusion in homogeneous and heterogeneous porous media (average of all tubes), using models in Figure 3.16.

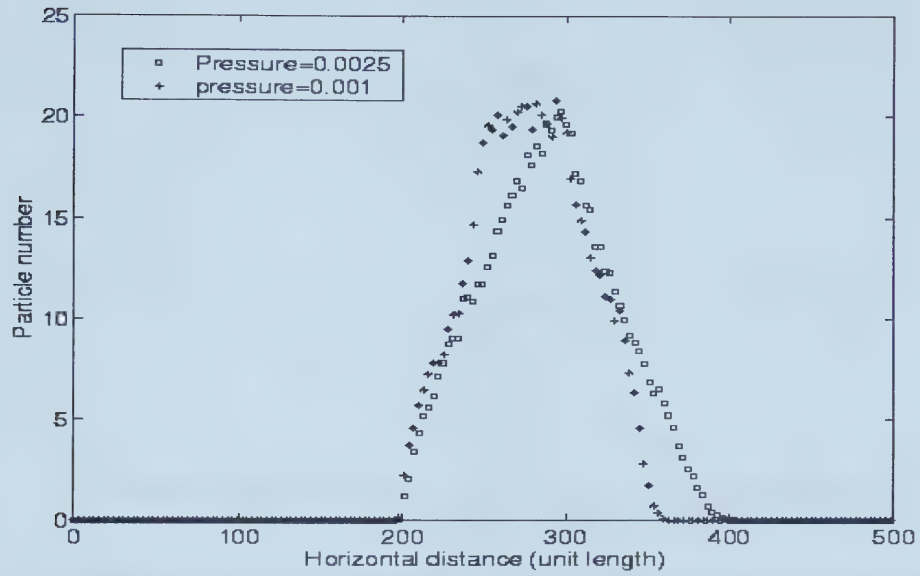


Figure 3.22 Dispersion in a homogeneous medium with a different pressure drop, using the model in Figure 3.16 (a), after 500 iterations.

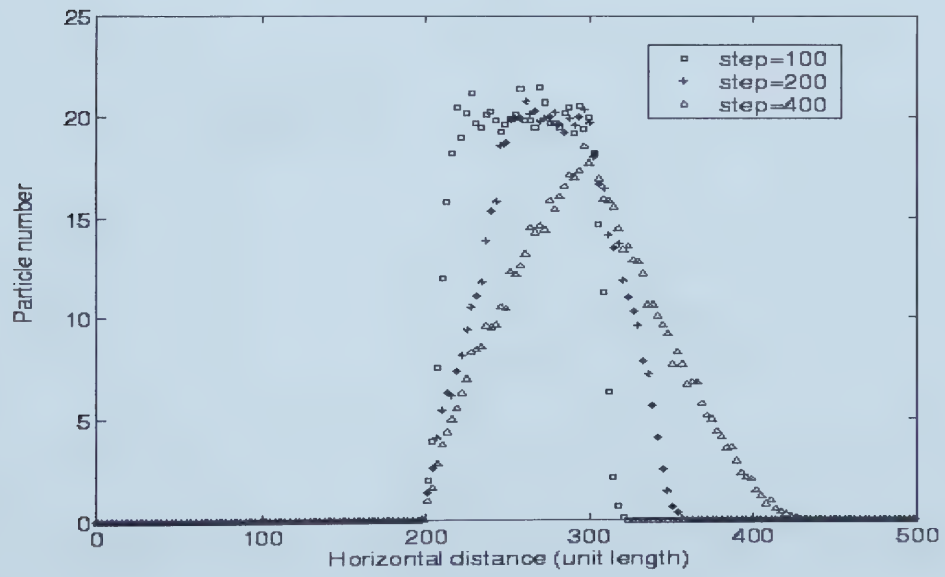


Figure 3.23 Dispersion in a homogeneous porous medium (average of all tubes), using the model in Figure 3.16(a).

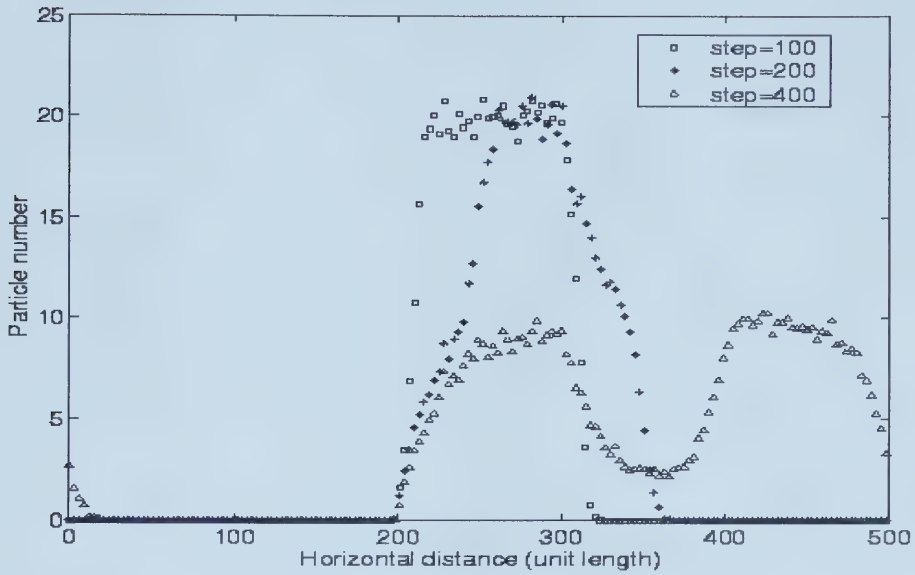


Figure 3.24 Dispersion in a heterogeneous porous medium (average of all tubes), using the model in Figure 3.16 (b).

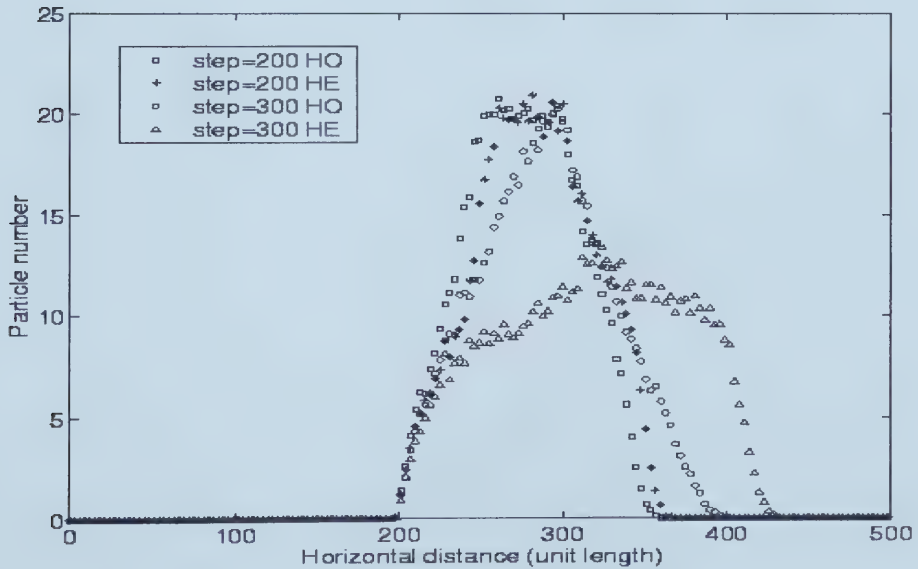


Figure 3.25 Comparison of dispersion in homogeneous and heterogeneous media (average of all tubes), using models in Figure 3.16.

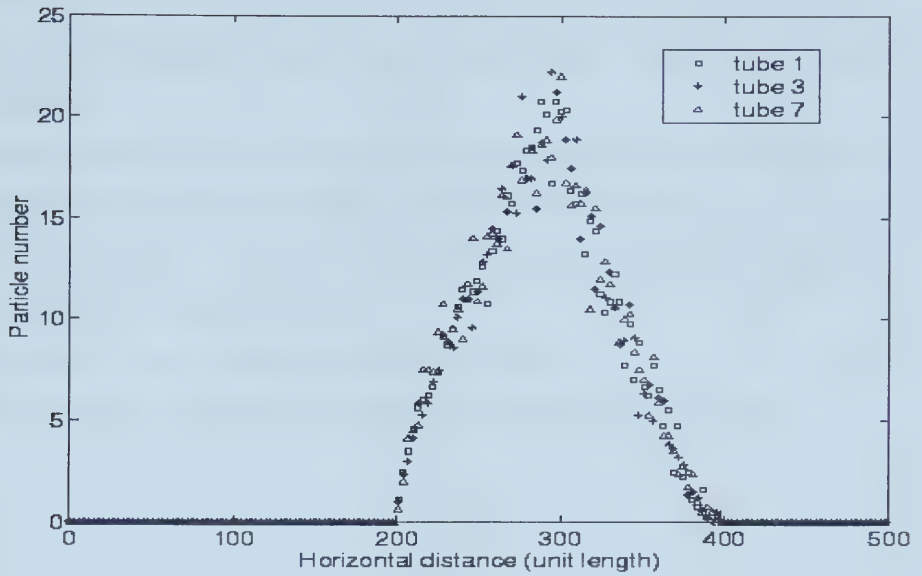


Figure 3.26 Dispersion in a homogeneous medium (specific tube averages), using the model in Figure 3.16 (a), after 300 iterations.

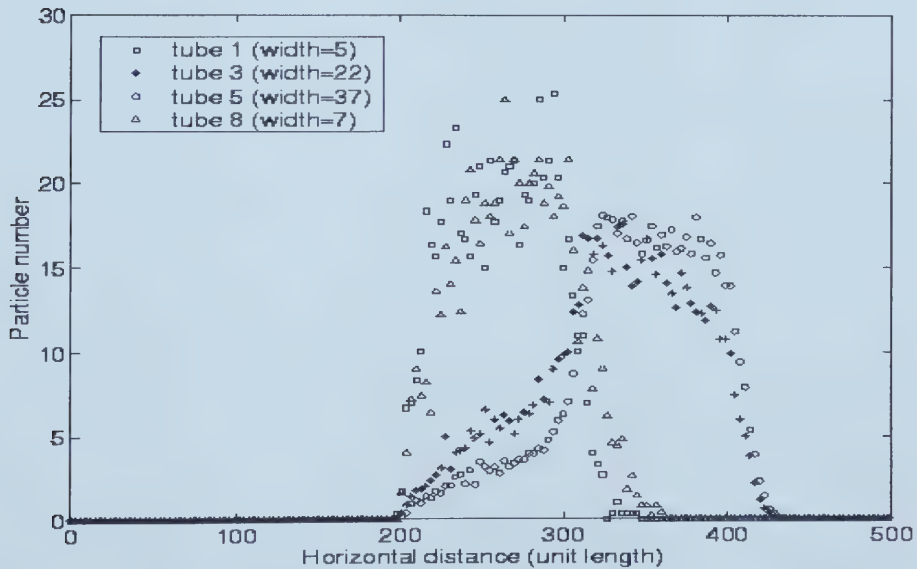


Figure 3.27 Dispersion in a heterogeneous medium (specific tube averages), using the model in Figure 3.16(b), after 300 iterations.

3.5.3 Concluding remarks

1. The thermodynamic automaton is an accurate way to model dispersion and diffusion in porous media.
2. For the same permeability, dispersion is faster in heterogeneous porous media than in homogeneous porous media, while diffusion is not affected as much.
3. In heterogeneous media, the dispersion is faster in large tubes than in small tubes, which causes separated dispersion peak.
4. Increasing pressure drop increases the dispersion process.
5. Complicated porous models may be modelled by using sophisticated tubes.

3.6 Wave propagation in porous media

3.6.1 Introduction

Seismic waves that propagate through the earth carry information about geological structures and rock properties. Seismic surveys record the continuous wavefield generated by impulsive sources that is reflected or transmitted by geological subsurface layers. Traditionally, the recorded data is processed to reveal some aspects of the subsurface geology. In recent years, geophysicists have started using seismic methods to evaluate and characterize hydrocarbon reservoirs and to monitor reservoir production and Enhanced Oil Recovery (EOR) processes (Aziz, et al, 1979). In these developments, numerical modelling is combined with the basic theory of seismic waves to provide the basis for understanding and interpreting seismic characteristics.

The environment of hydrocarbon reservoirs is a composite multiphase media with gas and/or liquid occupying the voids between solid grains. Seismic modelling methods, however, have generally treated the medium as a single-phase elastic solid or more often as a layered fluid. Seismic modelling using the acoustic or the scalar wave equation is probably the simplest example. In these modelling techniques, no direct correlations are established between the seismic characteristics and the fundamental bulk characteristics of reservoirs in spite of the well known fact that seismic wave amplitude, velocity, attenuation, and dispersion intrinsically depend not only upon the rock type but also upon the porosity, the properties of pore fluids, the confining pressure, and other factors.

Recently, the lattice gas based cellular automaton fluid method has been presented as a fast and efficient way for solving acoustic wave equations (Rothman, 1987; Huang, 1988; Jiao, 1996; Liu, 1997). However, some fundamental problems exist in this method when modelling wave propagation in a realistic model. Besides its intrinsic noisy character, one of the most serious drawbacks is the difficulty of extending the models from homogeneous to heterogeneous media. The other problems are difficulty in setting up different boundary conditions and confining the lattice to some specific area. Unless

these problems are resolved, thermodynamic automata can hardly be used as a useful tool for numerical seismic modelling or imaging. More work needs to be done in this area.

3.6.2 Theoretical background

Many authors contributed to the theory of seismic wave propagation in rock or porous media. Gassmann (1951) offers a formulation that approximates the wave propagation in porous, homogeneous rock if the material parameters are the appropriate averages of the rock's constituents. Biot (1962) on the other hand, offers a comprehensive theory that includes Gassmann as a special low-frequency case. de la Cruz and Spanos (1985,1989a, 1989b) offer equations that have a more satisfactory physical basis and use volume averaging to construct the macroscopic continuum equations which describe wave propagation in a porous solid filled with fluid. The final equations include viscous dissipation with the fluid element and the induced mass coefficient through its pore scale origin, Here only acoustic model is presented and modeled.

Acoustic model

Seismic P-waves can be approximated under the assumption of small-amplitude perturbations to the static state (Wapenaar and Berkhout, 1989). The equations of continuity and momentum can be rewritten to the following linear acoustic wave equations.

$$\frac{\partial[\Delta \rho(x, t)]}{\partial t} + \rho_0 \nabla \cdot v(x, t) = 0, \quad (3.42)$$

$$\rho_0(x) \frac{\partial v(x, t)}{\partial t} + \nabla[\Delta p(x, t)] = 0, \quad (3.43)$$

$$\Delta p(x, t) = C_s^2 \Delta \rho(x, t). \quad (3.44)$$

where $\rho_0(x)$ represents mass density; $p_0(x)$ represents the static pressure; $\Delta \rho(x, t)$ and $\Delta p(x, t)$ represent changes of mass density and pressure, respectively, which are caused

by the acoustic wave field; and C_s is referred to as the speed of sound. Similar to P and S waves, The attenuation of acoustic wave is functions of frequency.

3.63 Numerical model and simulation results

Three models have been constructed in order to analyze acoustic wave propagation in porous media. The parameters of the first mode are:

- (1) 100 x 100 lattice size; each cell contains 20 particles.
- (2) The initial particle speed is 0.1.
- (3) Top and bottom boundaries are assigned thermodynamic boundary conditions with β being 200.
- (4) A line seismic source is modelled by changing the particle speed as 5 times as the initial speed.
- (5) The source is placed along the x -axis at the bottom ($j=2$).
- (6) The receivers are placed along the y -axis.

The simulation results are presented in Figure 3.28. The selected receivers are at positions 2, 10, 15, 20 and 24; the total time is 500 time steps; the sampling rate is a unit time step. From observing the receiver response, it is clear that the acoustic wave propagates from one receiver to the other. The first arrival is stronger in the closest receiver and is attenuated as the wave propagates due to viscous dissipation. The speed of wave motion can be calculated. This reflects the dimensionless character of the automata.

In the second model, the initialization of the lattice is the same as the first, except that each cell contains 10 particles; the initial particle speed is 0.01; the particle speed at the source is set as a sinusoidal wave with maximum speed being 9 times bigger than the initial speed and 100 X 20 lattice cells are used as sources. Each iteration runs for 500 time steps. The amplitude versus position along the y -axis profile at different time steps is shown in Figure 3.29. One can notice the wave attenuation increases as distance from the source.

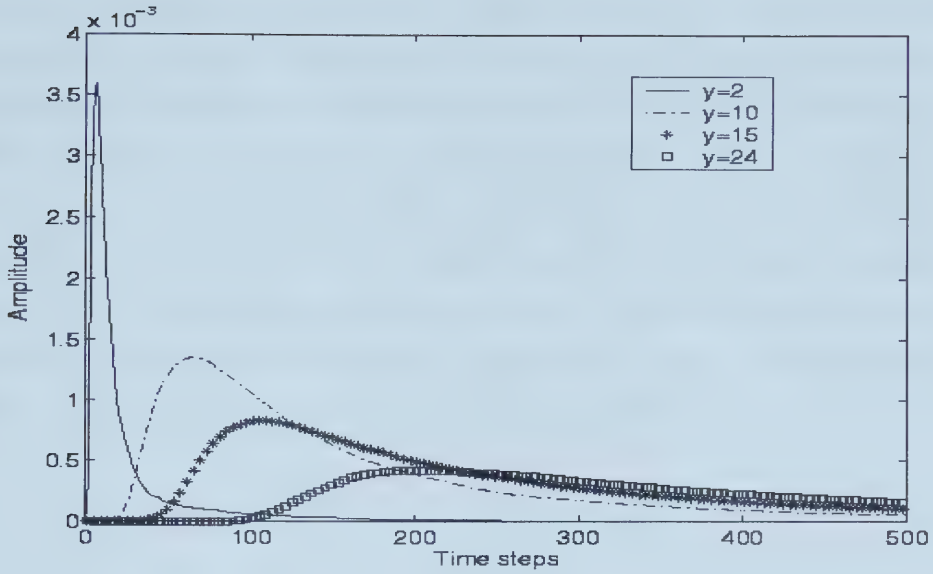


Figure 3.28 Lattice gas automaton simulation results of acoustic wave propagation. Lattice size: 100×100 ; sources are assigned on 100×2 cells; results drawn at 500th time step.

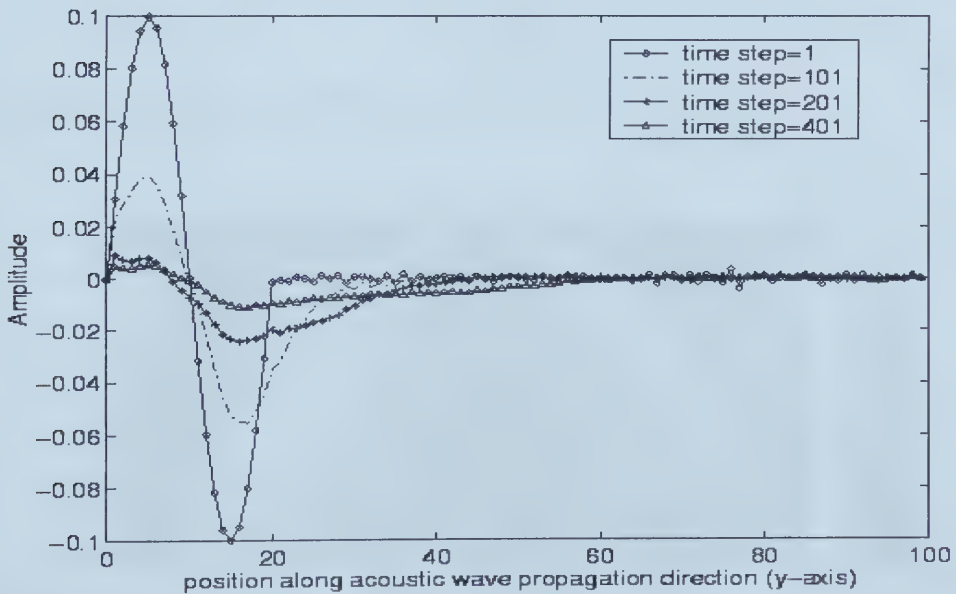


Figure 3.29 Lattice gas automaton simulation results of acoustic wave propagation. Lattice size: 100×100 ; sources are assigned on 100×20 cells with sine wave; results are obtained by averaging along each row.

The construction of the final model is also similar to the second one except that the lattice size is 100×40 ; two layers are assigned with one layer ($y \leq 20$) having 20 particles in each cell and 50 particles in each cell at the other layer. The source is a point at the middle of the bottom. The source and receivers are shown in Figure 3.30. Simulation results using a Common Shot Point (CSP) gather are shown in Figure 3.31. Though a hyperbolic curve of the first arrival is observed, one fails to get the reflection energy. Also the signal is noisy and the bandwidth is too large. The current thermal boundary condition models an absorbing boundary. Therefore, if one wants to attempt modelling seismic reflection and refraction, the model should be modified.

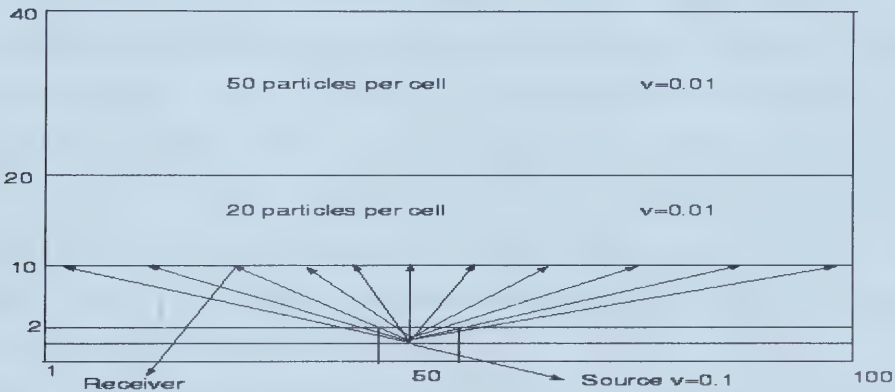


Figure 3.30 Diagram of common source and receivers configurations.

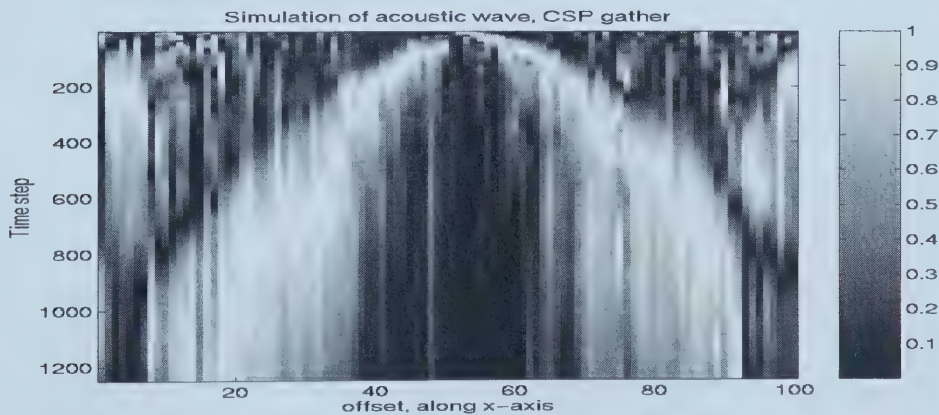


Figure 3.31 Lattice gas automaton simulation of acoustic Common shot point gather collected according to Figure 3.30. Black represents lower amplitude.

3.7 Summary

1. A 2D thermodynamic automaton model for modelling particle number distribution due to gravity was constructed. A thermal boundary condition was applied to four boundaries. The simulation results obey the Barometric formula.
2. Laminar flow and turbulence were simulated. The Reynolds number at the onset of turbulence was calculated. The particle velocity vectors clearly showed the difference between laminar and turbulent flow.
3. Heat convection was modelled by assigning a high temperature at the right boundary. The temperature of the other boundaries and the internal cells was the same. After a few iterations, heating effects could be observed from the velocity vectors.
4. Dispersion and diffusion in porous media were modelled and compared. The porosity was introduced by using a set of tubes. The heterogeneity was applied by adjusting the width of the tubes. Diffusion was less affected by the porous media (tube width) than dispersion. Dispersion occurred faster in bigger tubes than in smaller tubes, which caused separation of the dispersion process according to the width of the tube. Under the same permeability, the dispersion process is faster in heterogeneous porous media than in homogeneous porous media.
5. Finally, acoustic wave propagation was simulated in a very simple model. The motion of the wave can be observed. However, more rules should be added in order to model the acoustic wave in a complex model.

Chapter 4

Implementation of 3D thermodynamic automata

4.1 Introduction

In recent years, 2D cellular automata models have been developed through various approaches. It is natural to consider extending 2D models to the 3D domain. Many efforts have been done since d'Humières (1986b) first proposed a FCHC (Face-Centred-Hyper-Cubic) model to solve the problems in three dimensions. Many authors (Movig et al., 1989; Dubrulle et al., 1991; Gunstensen, 1991; Chen et al., 1991; Hénon 1992; Steacy et al., 1995) have contributed to the 3D lattice gas automata. There have been two main approaches for simulating 3D Navier-Stokes equations on lattices. They are: the FCHC based on a FHP model and the cubic model based on a 2D multi-speed model. However, most work has been done on the FCHC model. Presented here is a new strategy to construct 3D thermodynamic lattice gas model based on Udey et al's 2D model (1999), which has been described in Chapter 2. One of the advantages of this model is that the isotropy is independent of the lattice size and shape. Therefore, it is relatively straightforward to develop this 2D model in 3D using any shape. For simplicity, a cubic lattice has been used here. 3D model setup is the same as for 2D models, except that the following rules need to be revised: boundary conditions, collision rules, distribution rules and propagation rules.

4.2 Construction of 3D thermodynamic automata

4.2.1 Three dimensional coordinates system (cubic, sphere)

A cubic model is used for the 3D simulations of a fluid flow. However, spherical coordinates are used, as shown in Figure 4.1.

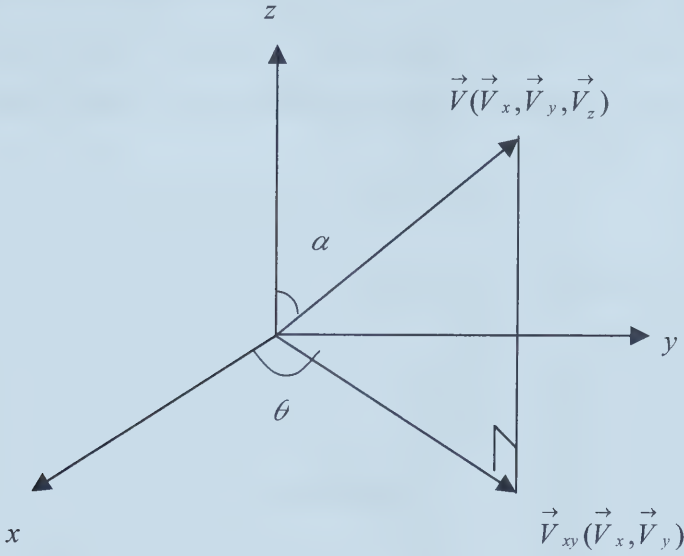


Figure 4.1 Diagram of spherical coordinate system used in the 3D thermodynamic automaton model

The relationship among \vec{V} , \vec{V}_{xy} , θ , α , \vec{V}_x , \vec{V}_y and V_z is described as follows:

$$\vec{V}_z = \vec{V} \cos \alpha \quad (4.1)$$

$$\vec{V}_{xy} = \vec{V} \sin \alpha \quad (4.2)$$

$$\vec{V}_x = \vec{V}_{xy} \cos \theta \quad (4.3)$$

$$\vec{V}_y = \vec{V}_{xy} \sin \theta \quad (4.4)$$

4.4.2 Collision, Propagation and motion rules

Unlike the 2D model, here the random number generators are used to generate two random numbers instead of one random number for each cell. These two random numbers decide the angle of θ and α , which control the particles direction of movement. The propagation of the particle is also determined by the probability of motion and the current particle speed. The probability is defined in equation (4.5)

$$\left. \begin{aligned} P_0 &= (1 - V_x)(1 - V_y)(1 - V_z) \\ P_{xyz} &= V_x V_y V_z \\ P_x &= V_x (1 - V_y)(1 - V_z) \\ P_y &= V_y (1 - V_x)(1 - V_z) \\ P_z &= V_z (1 - V_x)(1 - V_y) \\ P_{xy} &= V_x V_y - P_{xyz} \\ P_{yz} &= V_y V_z - P_{xyz} \\ P_{xz} &= V_x V_z - P_{xyz} \end{aligned} \right\}, \quad (4.5)$$

where V_x, V_y, V_z are the particle velocities along x, y, z direction respectively and they are all less than 0.0; P is the calculated probability, the subscripts of P represents eight possible directions in which the particles may move. The sum of all the above probabilities equals 1. The propagation rules depend on the generated probability P_{gen} and the calculated probabilities:

- (1) Particle stays if $P_{\text{gen}} < P_0$
- (2) Particle moves along x if $P_0 < P_{\text{gen}} < P_0 + P_x$
- (3) Particle moves along y if $P_0 + P_x < P_{\text{gen}} < P_0 + P_x + P_y$
- (4) Particle moves along z if $P_0 + P_x + P_y < P_{\text{gen}} < P_0 + P_x + P_y + P_z$
- (5) Particle moves along xy diagonal if $P_0 + P_x + P_y + P_z < P_{\text{gen}} < P_0 + P_x + P_y + P_z + P_{xy}$
- (6) Particle moves along yz diagonal if $P_0 + P_x + P_y + P_z + P_{xy} < P_{\text{gen}} < P_0 + P_x + P_y + P_z + P_{xy} + P_{yz}$

- (7) Particle moves along xz diagonal if $P_0 + P_x + P_y + P_z + P_{xy} + P_{yz} < P_{gen} < P_0 + P_x + P_y + P_z + P_{xy} + P_{yz} + P_{xz}$
- (8) Particle moves along xyz diagonal if $P_0 + P_x + P_y + P_z + P_{xy} + P_{yz} + P_{xz} < P_{gen} < P_0 + P_x + P_y + P_z + P_{xy} + P_{yz} + P_{xz} + P_{xyz} = 1$

The exact position of the particle is decided by a combination of the above rules and its current velocity. The particles collision is completed in a center-mass frame. The two angles, α (0° to 180°) and θ (0° to 360°), are generated for energy transformation during a collision.

4.2.3 Boundary conditions

Boundary conditions are assigned slightly different from the 2D model. When a particle hits a boundary in three-dimensional space, it bounces back according to boundary conditions. Suppose a particle hits a boundary (Figure 4.2), in the case of the non-slip or slip boundary condition, the particle will reverse the direction or reverse direction according to a reflection rule. For the thermodynamic boundary conditions, the particle will move back with the angle α (0° to 180°) and θ (270° to 360° or 0° to 90°) when it hits the left boundary; it will move back with the angle α (90° to 180°) θ (0° to 360°) when it hits the top boundary. Right, bottom, front, and back boundaries are assigned in a similar fashion.

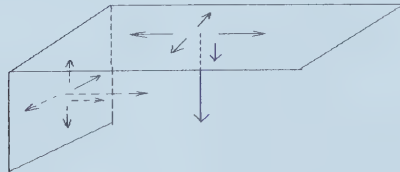


Figure 4.2 Diagram of particles hitting left and top boundaries

4.2.4 Codes revision

It was necessary to extensively modify the 2D code for the 3D case. The object-oriented style has been imitated in the C programming language using the Unix operating system. The boundary condition code has been totally changed. The collision and propagation code was slightly revised according to the rules for 3D. The density distribution function was calculated according to 3D calculus theory. Other parts, such as initialization of particles, cells, lattice, particle averaging, are simply extended from 2D to 3D. All simulations of 3D hydrodynamics are conducted using a Linux PC-686 computer. The applications are introduced in the following chapter.

Chapter 5

Applications of 3D thermodynamic automaton simulation

5.1 Introduction

In this chapter, models are constructed according to the rules stated in Chapter 4. First, thermal equilibrium state is modelled to check the validity of the 3D lattice gas model and then Darcy's empirical law of quasi-statistic flow and Poiseuille flow are simulated to further verify the model validity. In section 5.4, Particle number distribution due to gravity is modelled in 3D space, which indicates that isotropy is maintained in the model. Finally, diffusion in tubes and in a porous media are simulated and compared with analytical calculations. All simulations are consistent with theoretical predictions.

5.2 3D thermodynamic automaton simulation of the thermal equilibrium state

A 3D thermodynamic automaton model was constructed in the previous chapter. In this chapter, the model is checked for validity by simulating the thermal equilibrium state, for which analytic solutions are available.

5.2.1 Theoretical background

For lower particle speeds ($v=0.1$ or 0.2), the speed distribution of gas molecules in the thermal equilibrium state obeys the non-relativistic Maxwell-Boltzmann distribution. The following formulas describe the relationship between the probability density $P(E)$, which is the particle number within the energy range of $E+dE$ and the temperature.

$$P(E) = Ce^{-\frac{1}{kT}E} \quad (5.1)$$

If $\beta = \frac{1}{KT}$, and consider the normalization condition $\int_0^{\infty} P(E) dE = 1$, then obtains

$$C = \beta \quad (5.2)$$

Substituting equation 5.2 into equation 5.1 yields

$$P(E) = \beta e^{-\beta E} \quad (5.3)$$

Taking the natural logarithm on both sides of equation 5.3, the linear equation 5.4 results

$$\ln(P(E)) = \ln(\beta) - \beta E. \quad (5.4)$$

The plot of $\ln(P(E))$ versus E is a straight line with slope $-\beta$ and interception $\ln(\beta)$. Thus, once β is known, temperature T can be determined immediately and vice versa.

This 3D thermodynamic automaton system can evolve into thermal equilibrium after a certain number of iteration time steps. Therefore, it is possible to initially construct a thermal equilibrium state without destroying the properties of the lattice gas system. This can be implemented by initializing the Maxwell-Boltzmann distribution. A relationship between an unvaried random variable x which is in the interval $[0, 1)$ and an exponential variable E , can be established by requiring that their corresponding areas under their curves be the same (Press, et al., 1992). That is

$$\int_0^x u(t) dt = \int_0^E \beta e^{-\beta t} dt \quad (5.5)$$

where $u(t)$ is a uniform distribution in $[0, 1)$ and satisfies

$$\int_0^1 u(t) dt = 1 \quad (5.6)$$

Upon integration of equation 5.5 and rearranging the formula, one obtains

$$E = \frac{-\ln(1-x)}{\beta} \quad (5.7)$$

Here, one uses equation 5.7 to initialize the particle speeds; x is given by random generator and β is given by the temperature or average velocity.

5.2.2 Models and simulation results

A 3D cubic thermodynamic automaton model has been set up according to the rules presented in Section 4.2 and with a lattice size of $100 \times 10 \times 10$. Two different initial speed models have been used. Six particles with the same mass ($m=1$) and same speed ($v=0.1$ or $v=0.2$) are placed in each cell. The particles are assigned with random orientation. Six periodic boundaries are built. The simulation ran for 1000 time steps. The initial speed distribution is shown in Figure 5.1. The speed distribution after 1000 iterations is shown in Figure 5.2 which is consistent with the analytical solution. Figure 5.3 illustrates corresponding plots of $\ln(P(E))$ versus energy E for $m=1$ and $v=0.1$ and 0.2 , respectively. The plot of $\ln(P(E))$ versus E are straight lines with different slopes as predicted by equation 5.4. Temperature can be derived from the slope of the lines. However, at higher energies, scattered points are observed because only a few particles reach these high energies, while a large number of particles are required for a valid statistical analysis.

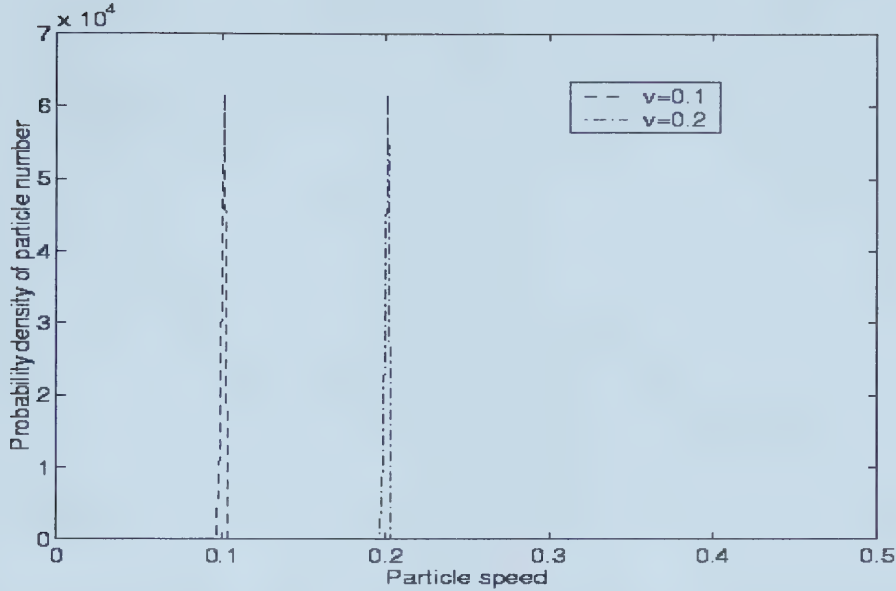


Figure 5.1 The initial simulation. Each particle has the same mass and speed $v=0.1$ or $v=0.2$ in two models respectively.

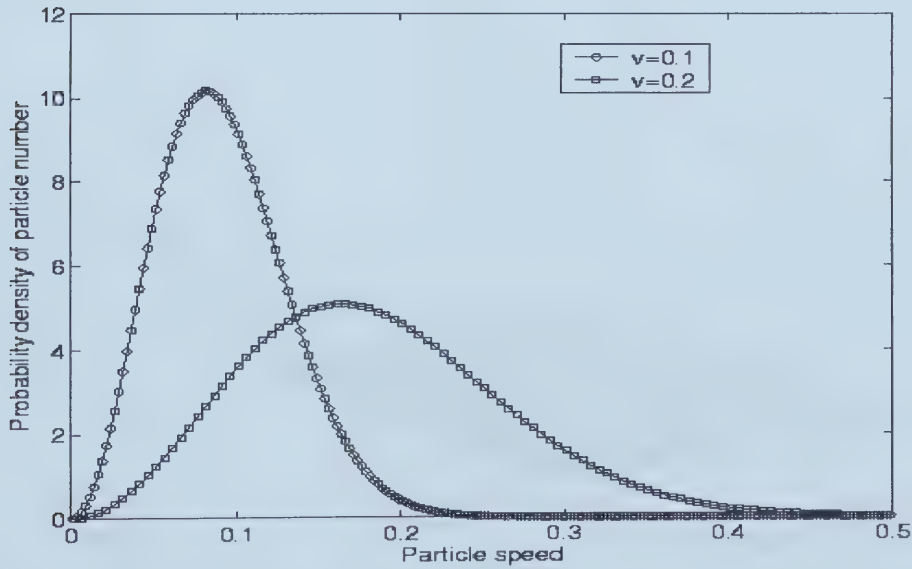


Figure 5.2 The particle speed distributions after 1000 iterations. 60000 particles have been assigned to $100 \times 10 \times 10$ lattice with the same mass and speed has been initialized randomly.

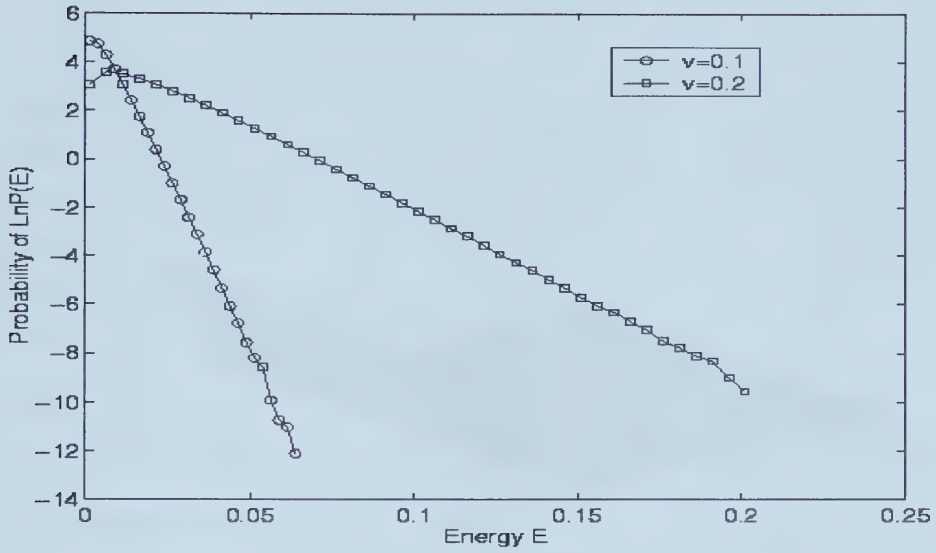


Figure 5.3 Corresponding plots of $\ln(P(E))$ versus energy E for the particle speed distribution with $v=0.1$ and 0.2 in Figure 5.2 for mass=1 after 1000 iterations.

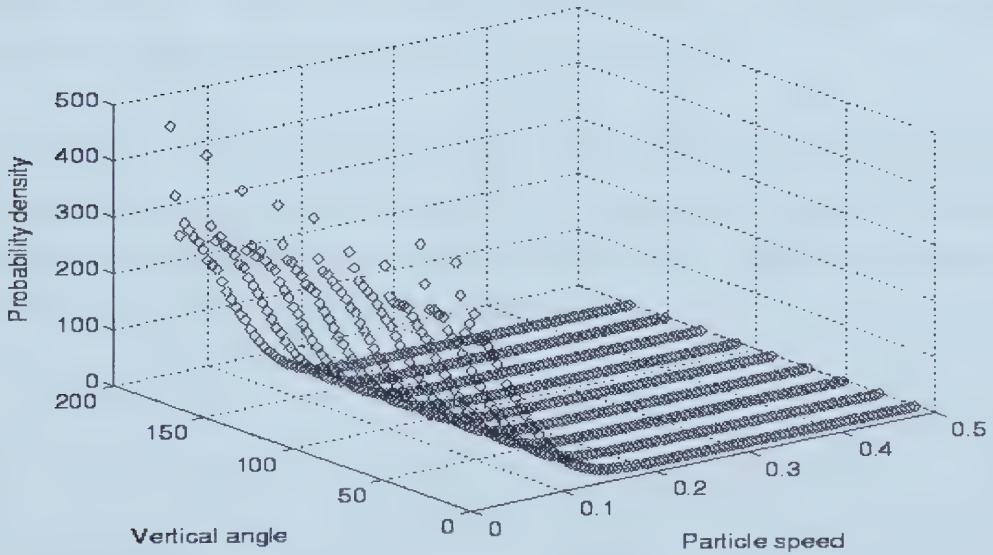


Figure 5.4 Sample plot of probability density of particles versus speed and vertical angle α . Selected section is obtained with horizontal angle θ equals 50° .

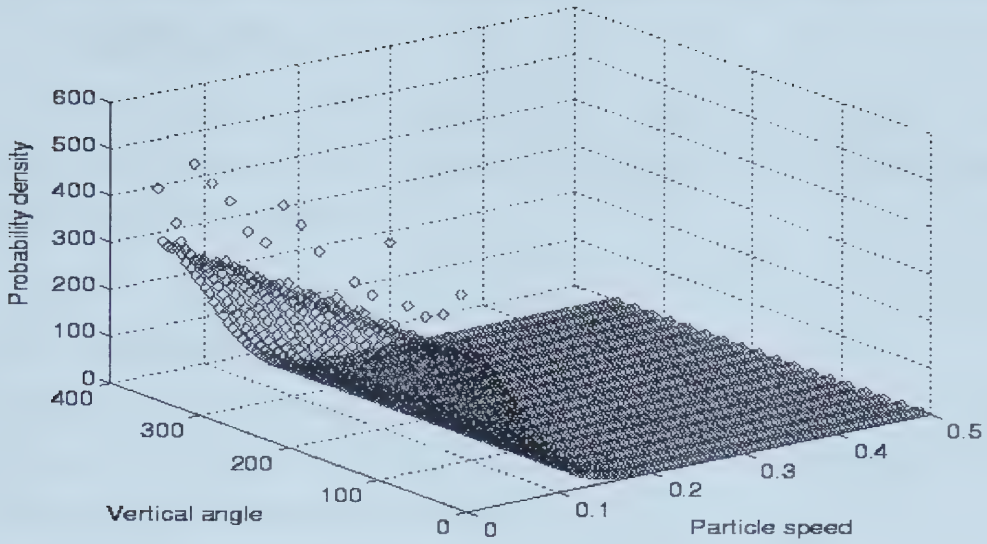


Figure 5.5 Sample Plot of probability density of particles versus speed and horizontal angle θ . Selected section is obtained when vertical angle α equals 50° .

Figure 5.4 and 5.5 show sample plots of density probability versus speed and angle with constant θ and α , respectively. Since the speed distribution is invariant with angle in both plots, it suggests that isotropy in the model is maintained.

The fact that the simulation results are in good agreement with the theoretical predictions not only provides support for the validity of the model, but also indicates that thermal effects are incorporated in the model. Temperature can be altered by changing the initialization of particle speeds and determined from β .

5.3 3D thermodynamic automaton simulation of Poiseuille flow and Darcy flow

In the Section 5.2, the validity of the model is verified. In this section, the 3D thermodynamic automaton model is modified to model Darcy flow in a porous medium and Poiseuille flow in a square pipe.

5.3.1 Theoretical background

The underlying theory of Darcy's law for 2D case was stated in section 3.4. Equation 3.6 still holds in a 3D porous medium. The following is pipe flow theory for both 2D and 3D case, quoted from Landau and Lifshitz (1959).

First, consider a 2D pipe with steady flow between two parallel planes in the presence of a pressure gradient. One takes one of these planes as the xy -plane, with the x -axis in the direction of the motion of the fluid. Since it is clear that velocity depends on y , the Navier-Stokes equations for this case are

$$\frac{\partial^2 v}{\partial y^2} = \frac{1}{\eta} \frac{\partial P}{\partial x} \quad (5.8)$$

$$\frac{\partial P}{\partial y} = 0 \quad (5.9)$$

where v is fluid flow velocity, η is fluid viscosity, and $\frac{\partial P}{\partial x}$ is the pressure gradient along x -axis which is assumed constant here. The solution of equations 5.8 and 5.9 is

$$v = \frac{1}{2\eta} \frac{dP}{dx} y^2 + ay + b \quad (5.10)$$

The coefficients a and b can be determined from boundary conditions, $v = 0$ for $y = 0$ and $y = h$. The result is

$$v = -\frac{1}{2\eta} \frac{dP}{dx} \left[\frac{1}{4} h^2 - \left(y - \frac{1}{2} h \right)^2 \right]. \quad (5.11)$$

Thus, the velocity varies parabolically across the fluid, reaching its maximum value in the middle.

Now, consider steady flow in a 3D pipe. One takes the pipe axis as the x -axis. Therefore fluid velocity is along the x -axis at all points, and is a function of y and z only. The Navier-Stokes equation gives

$$\frac{\partial^2 v}{\partial y^2} + \frac{\partial^2 v}{\partial z^2} = \frac{1}{\eta} \frac{dP}{dx}, \quad (5.12)$$

$$\frac{\partial P}{\partial y} = \frac{\partial P}{\partial z} = 0. \quad (5.13)$$

One can solve the above equations for a pipe of circular cross section. In this case, taking the origin at the center of the circle, using polar coordinates, and using boundary conditions that $v = 0$ when $r = R$, one gets

$$v = -\frac{\Delta P}{4\eta l} (R^2 - r^2). \quad (5.14)$$

Equation 5.14 shows that the velocity across the pipe is parabolic.

For a square model, the solution of equations 5.12 and 5.13 is more complicated. However, one can still expect to get a parabolic velocity distribution across the yz plane.

5.3.2 Models and simulation results

The lattice size used is $30 \times 10 \times 10$. The initial particle speed is assigned according to the thermal equilibrium state for which the average particle speed equals 0.1. Periodic boundary conditions are assigned to the left and right boundaries. A constant pressure gradient $P=0.0001$ can be added along the x-axis direction of the fluid motion. Thermodynamic boundary conditions are set up on the other four boundaries with $\beta=200$. For the simulation of Poiseuille flow, no permeability is introduced. For the simulation of Darcy flow, permeability is incorporated by setting the probability of solid-fluid collision to 0.3. The simulation results are obtained after 5000 time iterations.

The sets of straight lines in Figure 5.6 show that flow rates are the same, which indicate that Darcy's law is valid in the modelling. These lines also indicate that isotropy is maintained in this model. In Figure 5.7, both theoretical expectation and numerical results are presented. It is noted that in Figure 5.7 (b), the numerical results matches the theoretical value much better than in Figure 5.7 (a) which shows that the simulation results converged with the time. Also for numerical results, each parabolic line has a different radius with the maximum in the middle position. In fact, the maximum is exactly in the middle of the pipe, which is where one would expect.

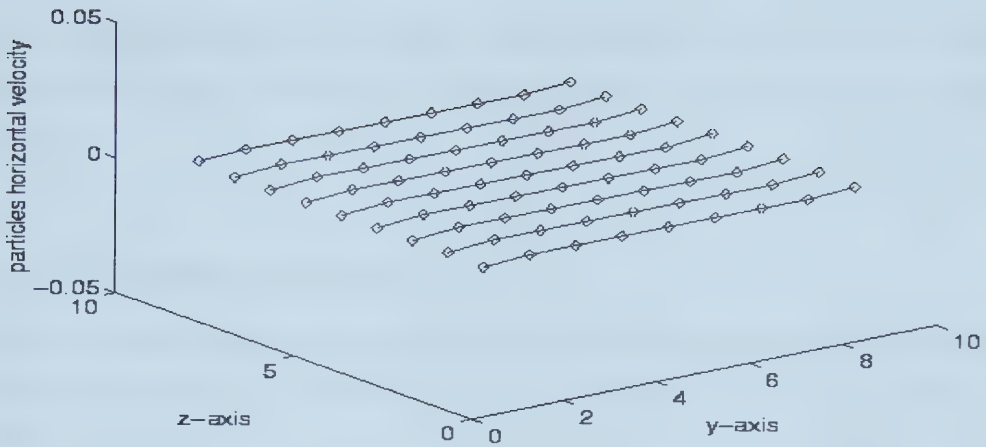


Figure 5.6 Darcy flow velocity profile for a square pipe cross-section at yz plane. 3D lattice gas simulation after 5000 time steps.

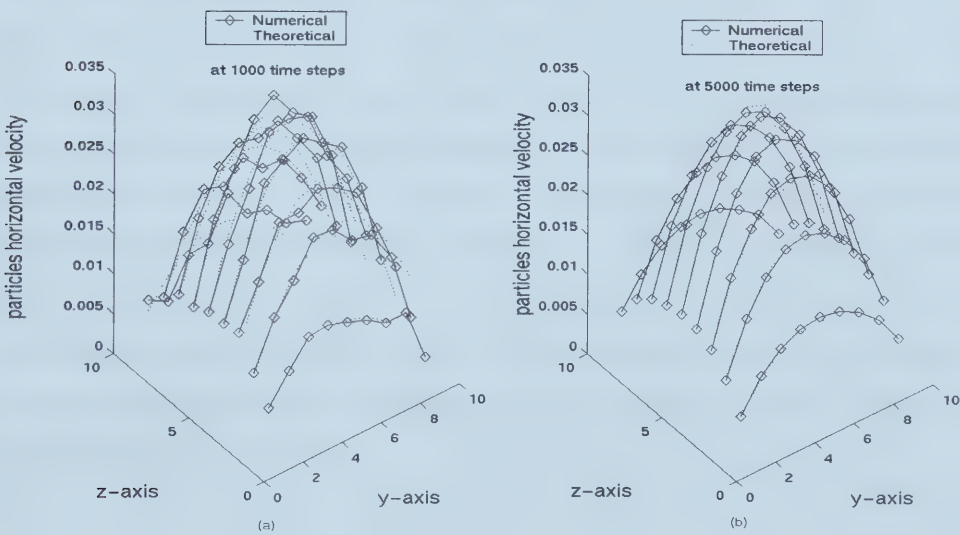


Figure 5.7 Poiseuille flow velocity profile for a square pipe cross-section at yz plane.

Dash line represents theoretical calculation, Solid line represents numerical result.

(a) Results after 1000 time steps, (b) Results after 5000 time steps.

5.4 3D thermodynamic automaton simulation of particle number distribution due to gravity

Here, the particle number distribution obeying Barometric formula due to gravity is modeled in 3D space. The results at the cross sections in the yz plane and xz plane are shown.

5.4.1 Theoretical background

The well-known theories about 2D particle number distribution were presented in Section 3.2.1. Because the gravity force will still act in only one direction, the final Barometric formula will remain unchanged for the 3D case. The exponential curve of particle distribution can be constructed analytically.

5.4.2 Model and Simulation results

A 3D cubic lattice gas model is constructed with a size of $100 \times 11 \times 12$. Each cell contains 50 particles. The speed of the particles is initialized according to the Maxwell-Boltzmann's distribution, with an average velocity of 0.1. Thermodynamic boundary conditions are assigned to all six boundaries with temperatures the same as the internal temperature. The force of gravity is applied by adding pressure along the x -axis direction to each particle for each time step. The results after 5000 iterations are presented in Figure 5.8 and Figure 5.9. Figure 5.8 is obtained from a cross-section at $z=5$ and Figure 5.9 is obtained from a cross-section at $y=5$. The exponential curves in both figures look the same, which might indicate that isotropy is maintained in the model. The results also match the theoretical solutions.

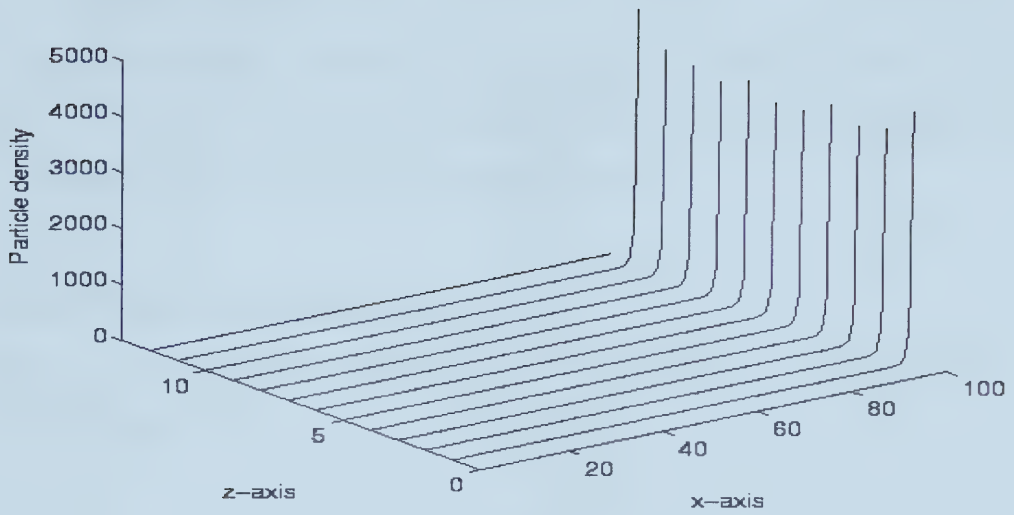


Figure 5.8 3D thermodynamic automaton simulation of the Barometric formula. Cross-section of the xz plane at $y=5$.

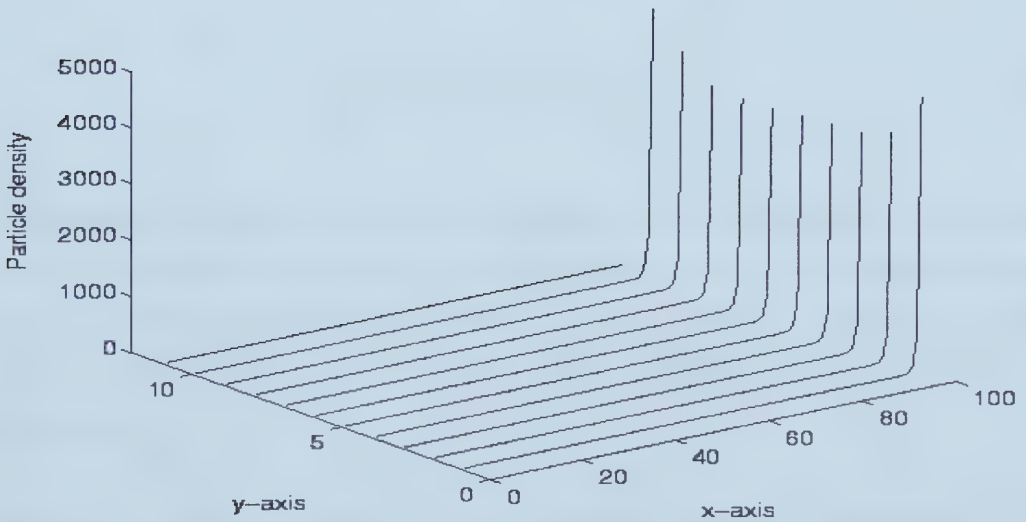


Figure 5.9 3D thermodynamic automaton simulation of the Barometric formula. Cross-section of the xy plane at $z=5$.

5.5 3D thermodynamic automaton simulation of diffusion in porous media

In this section, lattice gas models are formed to simulate the diffusion in different media such as a tube medium or heterogeneous porous medium. The simulation results are then compared with each other and with the analytical solutions.

5.5.1 Theoretical background

As stated in Chapter 3, the diffusion process in the one-dimension can be described by the following equation:

$$\frac{\partial c}{\partial t} = D \frac{\partial^2 c}{\partial x^2}, \quad (5.15)$$

where c is the concentration of the fluid undergoing diffusion, D is the diffusion coefficient, and t is the time. A solution to equation 5.15 is

$$c = \frac{1}{(4 \pi D t)^{\frac{1}{2}}} \exp\left(-\frac{x^2}{4 D t}\right). \quad (5.16)$$

The analytic solution to the evolution of concentration c with the parameter Dt being 0.01, 0.02, 0.03, 0.05, 0.07, 0.09, 0.1, 0.2, 0.3, 0.5, 0.7, 0.9, 1, 2, 3, 5, 7, and 9 are plotted in Figure 5.10. It is noted that for constant D and each time t , the concentration profile has a bell shape. Figure 5.10 also indicates that the concentration profile will flatten out with the time.

The apparent diffusion coefficient D_a is used instead of D if the diffusion occurs in a porous medium. The apparent diffusion coefficient D_a is related to the permeability (K) of the porous medium according to equation 5.17 (Barrer, 1951)

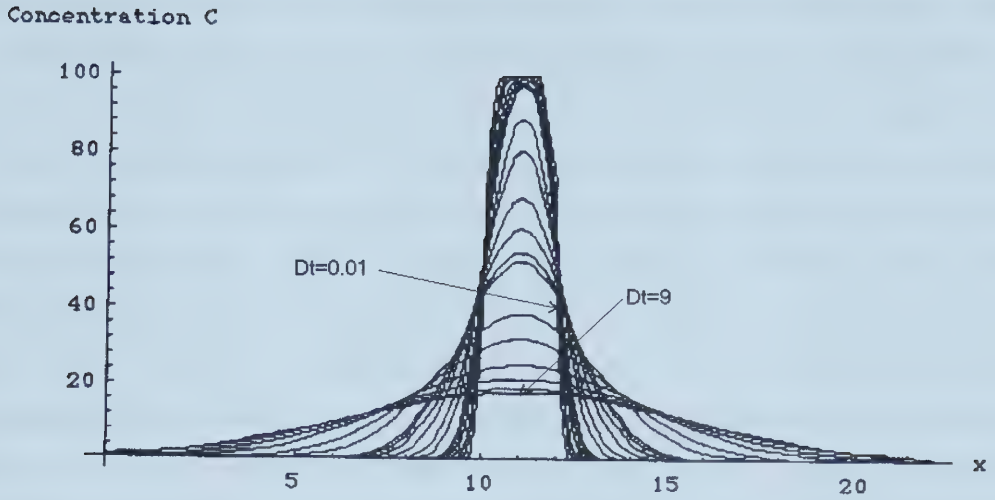


Figure 5.10 Analytic solution to the evolution of concentration c using Mathematica for the given values of the parameter Dt of 0.01, 0.02, 0.03, 0.05, 0.07, 0.09, 0.1, 0.2, 0.3, 0.5, 0.7, 0.9, 1, 2, 3, 5, 7 and 9 (Yang, 1996)

$$K = -D_a \frac{\partial c}{\partial x}. \quad (5.17)$$

The fact that molecular coefficient D measured in a tube is larger than the apparent diffusion coefficient D_a in a porous medium indicates that the diffusion process occurs faster in a tube.

5.5.2 Models and simulation results

A few models are constructed. The common features of these models are: lattice size $200 \times 10 \times 7$, corresponding to the x , y and z direction, respectively; 100 particles reside in each cell; the initial particle speed is 0.1; two or three types of species are assigned with one species being taken as tracing particles; The temperature for the boundary is set

according to $\beta=200$; The simulations run for 1000 time steps. First, two testing models with periodic or thermodynamic boundary conditions are used. The configurations of the models are as follows: The lattice is separated into two parts at the middle of x-axis with the tracing particles in the right half of the lattice. The solid-liquid collision probability is 0.0. Thus, diffusion in a square tube is modelled. The mass of both types of particles is 1.0. All results are plotted in 2D xz cross-sections by averaging along the y -axis direction. The results in Figure 5.11 show diffusion profiles with periodic boundary conditions, while the results in Figure 5.12 display a diffusion profiles with thermodynamic boundary conditions. Graphs in both figures indicate an exponential curve which matches the analytical solution in equation 5.16. However, for the model simulation with a periodic boundary, the fluid (Figure 5.11) diffuses across the boundary to the reverse side, making the diffusion process hard to identify. Therefore the model is modified to have thermodynamic boundary conditions as in Figure 5.12, it is noted that the diffusion occurs with time and distance from the original states.

One has observed diffusion happening in the above models and the model will now be modified to conduct further simulations. In order to better compare the simulation results with some symmetry, tracing particles are put into the middle of the square tube or a porous box in latter models. All boundary conditions are periodical, which allow the particles to flow cycling. For a homogeneous porous media, the porosity is introduced by changing the solid-liquid collision probability from 0 (tube) to 0.1. Heterogeneity is applied by randomly varying the solid-collision probability (SP) in space according to the Double-Boltzmann function with the average SP being 0.588. The simulation results of diffusion in the tube and in the homogeneous porous media are plotted in Figure 5.13 and Figure 5.14, respectively. They both show a clear bell shape. The almost identical curve in both figures indicates that isotropy is maintained during the simulations and that assigning the same SP of 0.1 or 0.588 to each cell is a good approach to introduce permeability. The results are in good agreement with the theoretical expectations. The simulation results in Figure 5.15 show that the diffusion processes occur faster in some cross-sections and slower in others. The symmetry of the diffusion profile does not hold any more. This is reasonable because the porosity varies with space.

Finally, comparisons of the simulation results after 1000 iterations for different media are presented in Figure 5.16. One can note that diffusion in a tube occurs faster than it does in homogeneous media in any cross-section and even faster in heterogeneous porous medium except in cross-section $z=1$. The results in Figure 5.16 also reveal that diffusion occurs faster in higher permeabilities (less SP) than in lower permeabilities for heterogeneous medium. These results also match the theoretical solutions.

Selected porous structures in heterogeneous case ($SP=0.588$) for two outstanding cross-sections at $z=1$ where diffusion occurs faster and at $z=2$ where diffusion occurs slower are presented in Figure 5.17. However, because of the complexity of the porous structure it is hard to explain from Figure 5.17 why diffusion happens faster in one section and slower in the others.

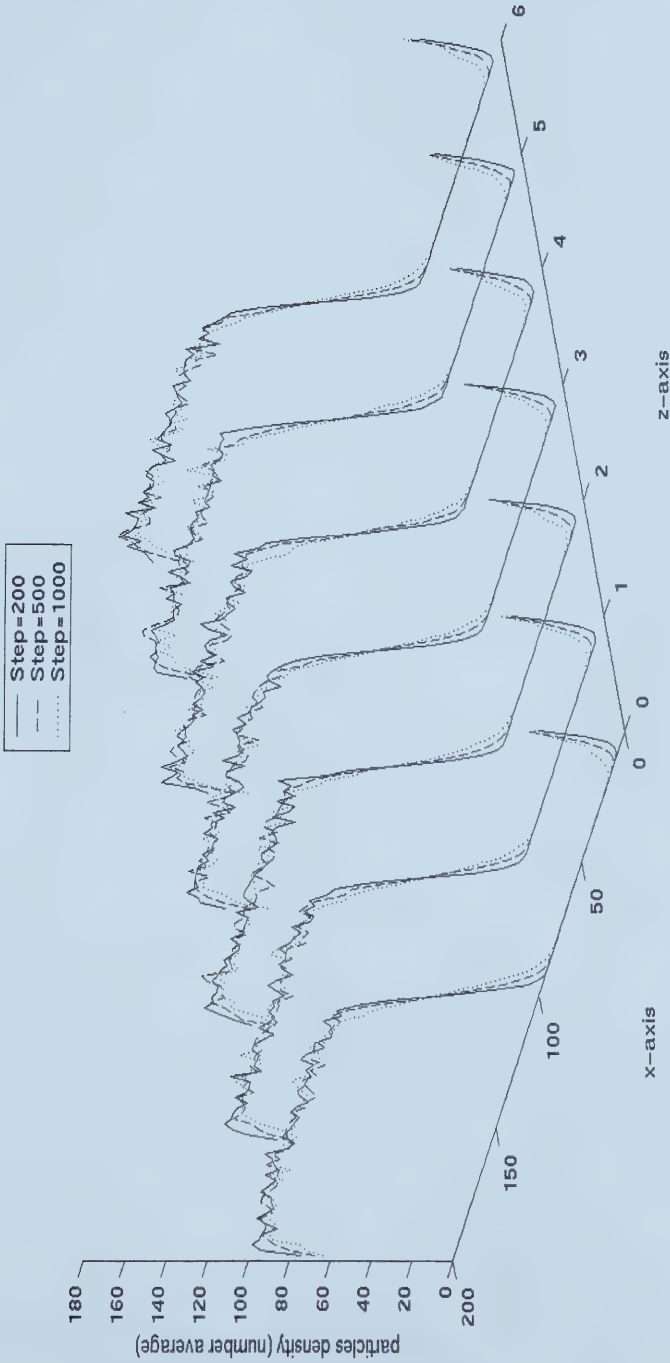


Figure 5.11 3D modelling of the diffusion process in a tube with periodic boundary conditions. The results are plotted after 2000 time iteration using a lattice size of $100 \times 10 \times 7$, 100 particles in each cell with speed initialized from Maxwell-Boltzmann distribution at $v=0.1$. The tracing particles are arranged in the right half of the cubic tube.

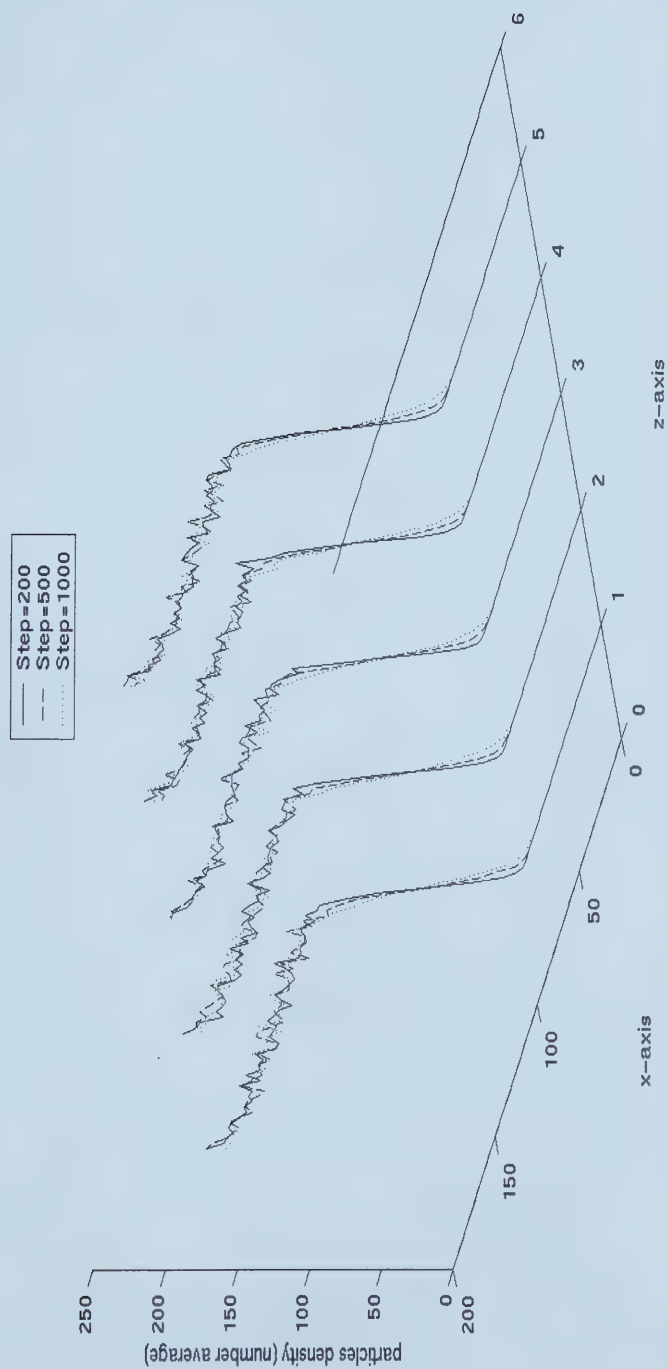


Figure 5.12 3D modelling of the diffusion process in a tube with thermodynamic boundary conditions. The result are plotted after 2000 time iteration using a lattice size of $100 \times 10 \times 7$, 100 particles in each cell with speed initialized from Maxwell-Boltzmann distribution at $v=0.1$. The tracing particles are arranged in the right half of the cubic tube.

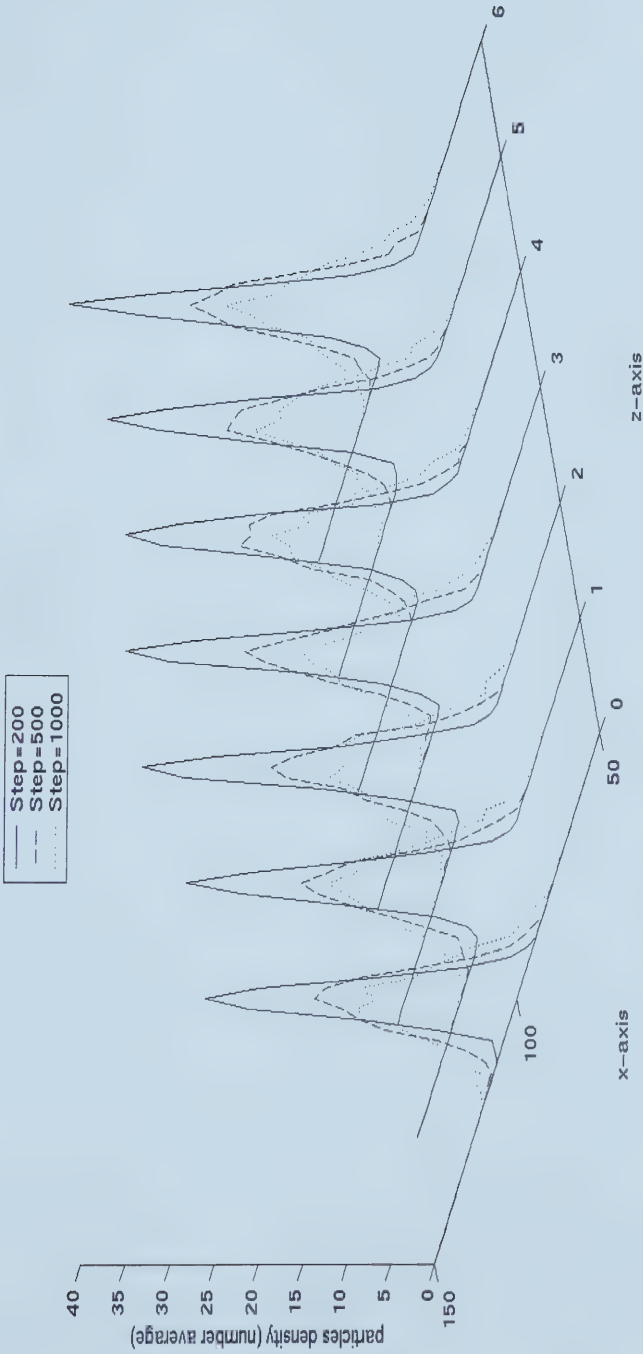


Figure 5.13 3D modelling of the diffusion process in a tube with periodic boundary conditions. The results are plotted after 1000 time iteration using lattice size of $100 \times 10 \times 7$, 100 particles in each cell with speed initialized from Maxwell-Boltzmann distribution at $v=0.1$. The tracing particles are arranged into middle part of the square tube along the x -axis direction. The remaining sides are assigned with two identical species.

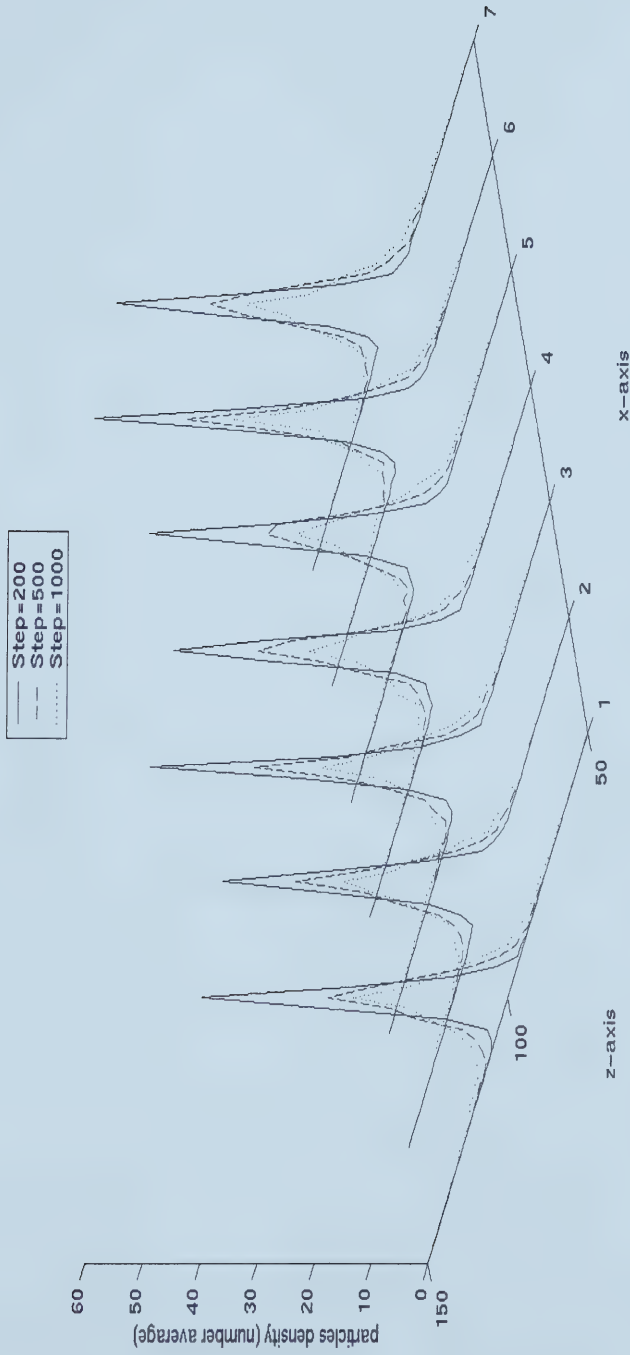


Figure 5.14 3D modelling of the diffusion process in homogeneous porous media with periodic boundary conditions. The results are plotted after 1000 time iteration using lattice size of $100 \times 10 \times 7$, 100 particles in each cell with speed initialized from Maxwell-Boltzmann distribution at $v=0.1$. The tracing particles are arranged into middle part of the cubic tube along x-axis direction. The rest sides are assigned with two identical species. The homogeneous porosity is introduced by setting the solid-liquid collision probability to 0.1.

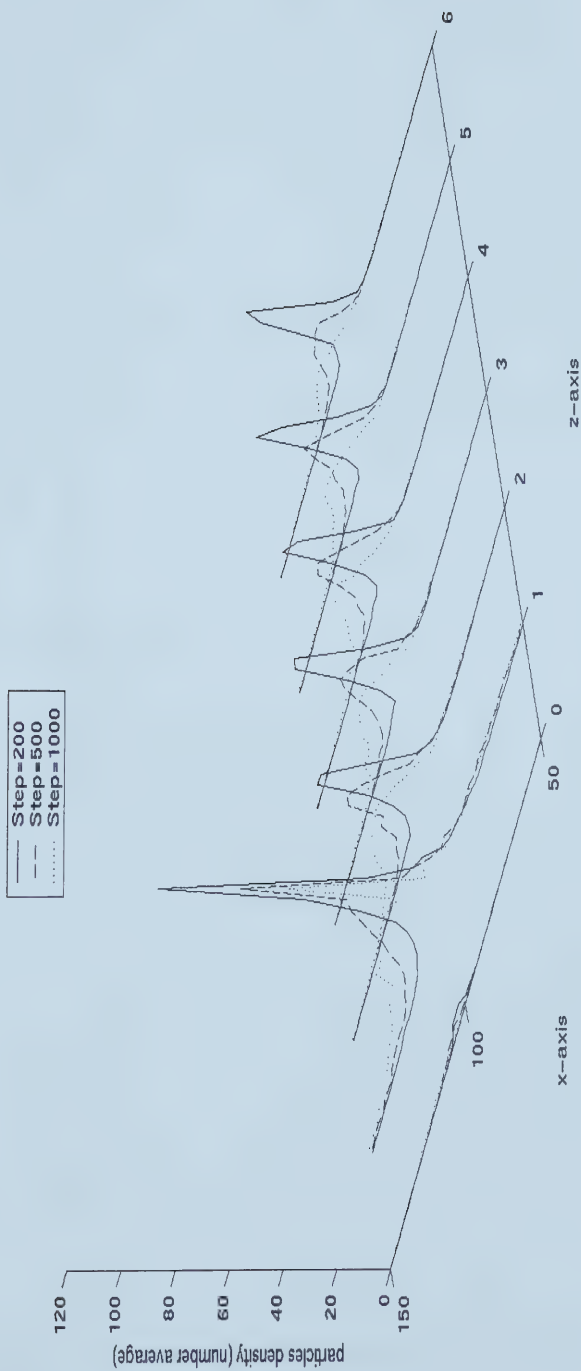


Figure 5.15 3D modelling of the diffusion process in heterogeneous porous media with periodic boundary conditions. The results are plotted after 1000 time iteration using lattice size of $100 \times 10 \times 7$, 100 particles in each cell with speed initialized from Maxwell-Boltzmann distribution at $v=0.1$. The tracing particles are arranged in the middle part of the cubic tube along x-axis direction. The two sides are assigned two identical species. The heterogeneous porosity is introduced by randomly allowing solid-liquid collision probability according to the Double-Boltzmann function with an average solid-liquid collision probability equaling 0.588.

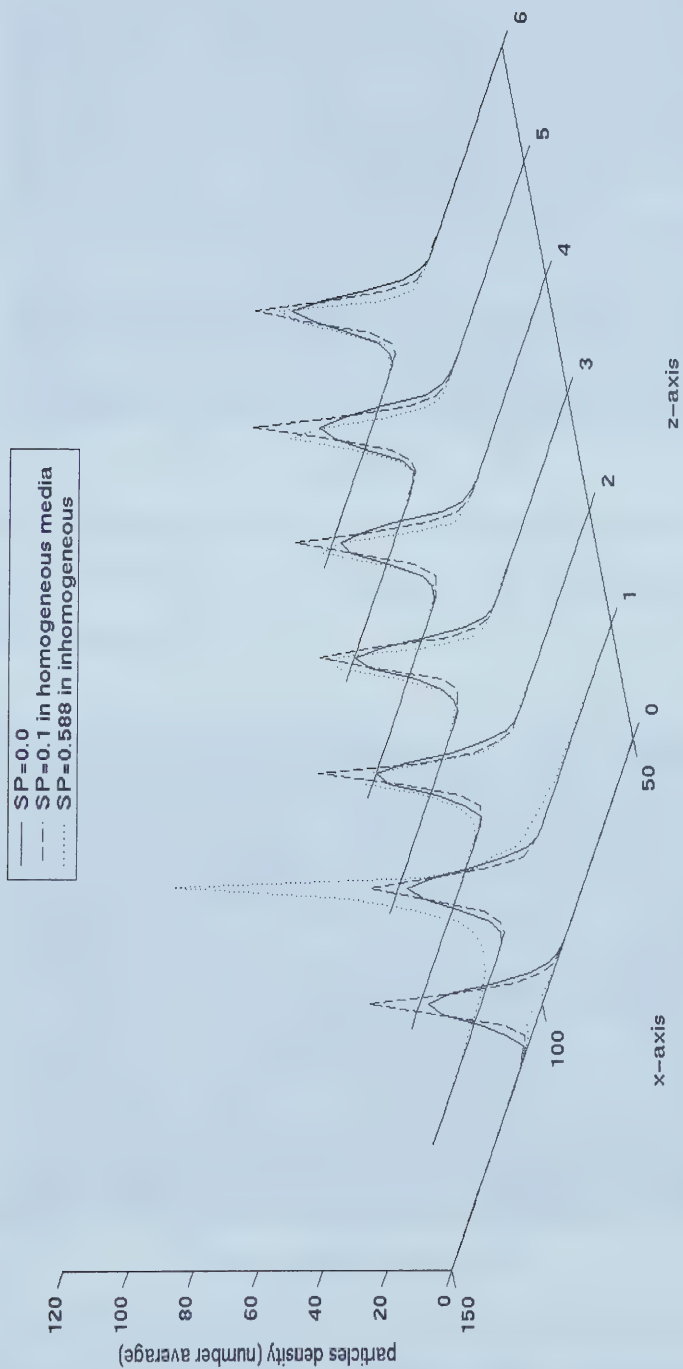


Figure 5.16 Comparisons of diffusion processes in tube, homogeneous porous media, and heterogeneous porous media. The lattice set up is the same as in Figure 5.13, 5.14, and 5.15 respectively. Selected profiles are the results after 1000 iterations.

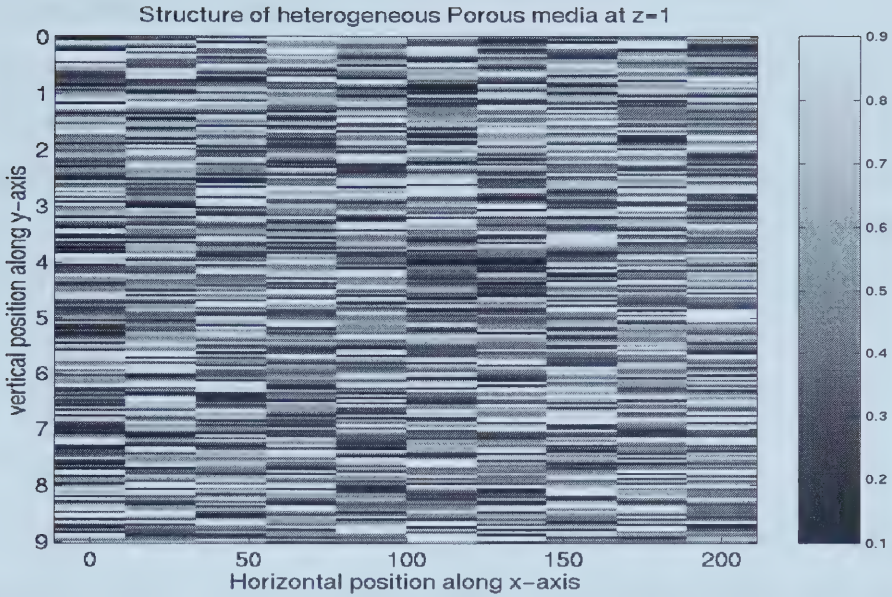


Figure 5.17 (a) Porosity structure in a heterogeneous porous medium in cross-section xy at $z=1$. Dark colours represent high permeability; lighter colours represent lower permeability.

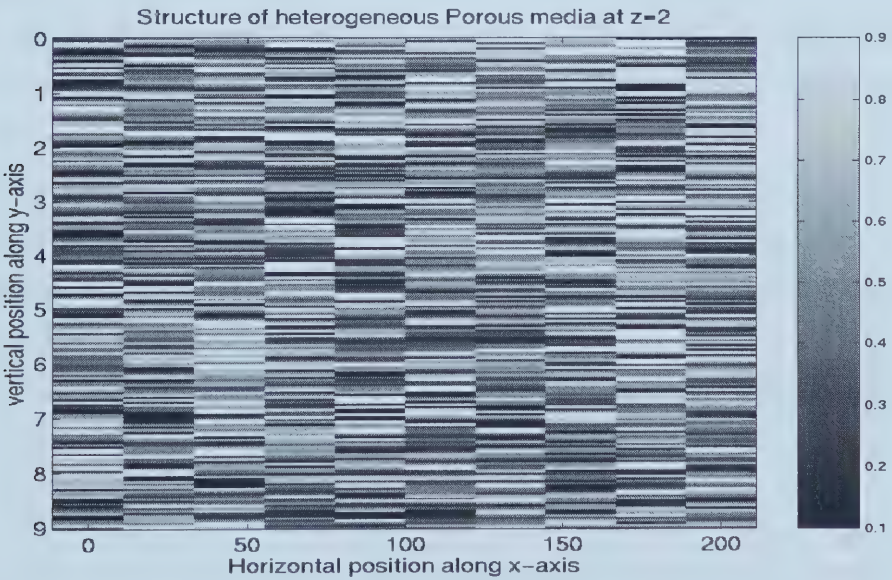


Figure 5.17 (b) Porosity structure in a heterogeneous porous medium in cross-section xy at $z=2$. Dark colours represent high permeability; lighter colour represent lower permeability.

5.5.3 Concluding remarks

In Section 5.5, models are constructed to simulate diffusion processes in different media. The results show that these models are effective at modeling diffusion. The diffusion is affected by the permeability. It turns out that diffusion in a tube is faster than in a porous medium and that diffusion occurs quicker in a porous medium with higher permeability. The diffusion profile in a heterogeneous medium is no longer symmetric and the speed of diffusion depends on the porosity structure.

5.6 Summary

1. The thermal equilibrium state in 3D space was simulated by the thermodynamic automaton model. The simulation results were consistent with the theoretical predictions, thus providing support for the validity of the model.
2. Darcy's law was verified by introducing porosity and a constant pressure drop into the 3D thermodynamic model. Poiseuille flow was also successfully simulated in the tube model.
3. The profile of the particle number distribution due to gravity was modelled in 3D space. The results match well with the Barometric formula, which is the analytical solution.
4. Diffusion processes in different media were tested. The results of the cross-sections showed that diffusion occurs faster in a tube than in a porous medium and that diffusion happens quicker in the medium with higher permeability than it does in low permeability medium.
5. The construction of the 3D thermodynamic automaton model is a success. Simulations of 3D fluid flow can be simulated using this model.

Chapter 6

Summary, conclusions and recommendations

A literature review of the evolution of cellular automata and lattice gas methods was presented in Chapter 1. Two approaches to modelling the Navier-Stokes equation are lattice gas automata and the lattice Boltzmann automata. Cellular automata have played an important role in the numerical simulation of hydrodynamics. The rules for constructing 2D square thermodynamic automaton model for the simulation of fluid flow has been described in Chapter 2.

The ability to describe the physics of fluid flow using a thermodynamic automaton model is verified in Chapter 3. In that chapter, models are constructed according to the rules in Chapter 2. First, the particle number distribution of the Barometric formula was modelled. Laminar and turbulent flow were studied to show the conditions for the onset of turbulence. Heat convection was also simulated by increasing the temperature in the right boundary of the box. It is noted that the model successfully describes temperatures both inside and at the boundary. Furthermore, it is interesting that one can introduce porosity by using a number of tubes and bring in heterogeneity by varying the size of the tubes. Dispersion and diffusion were described using this model. It shows that dispersion propagates more quickly in big tubes than in small tubes and that with the same permeability, dispersion occurs to a greater extent in a heterogeneous porous medium than it does in homogeneous porous media. Finally, the simple models for simulating acoustic wave propagation were built to monitor the motion of the acoustic waves. However, presently no method is capable of numerically modelling seismic waves through rocks with realistic microscopic features such as complex rock matrices, or fractures system.

The 2D thermodynamic automaton model was extended into 3D space. The revised rules were listed in Chapter 4. Applications of 3D cubic thermodynamic automata models were presented in Chapter 5. The validity of this model was first verified by the simulation of thermal equilibrium states in cubic models and was later verified by the simulation of

Darcy's law and Poiseuille flow. The isotropy is easily maintained in this model. By changing solid-liquid collision probabilities in space, one can incorporate permeability into the cubic model. The comparison of diffusion in different media shows that these 3D thermodynamic models are capable of simulating fluid flow in complex media such as in heterogeneous porous media

In these models, the assumption that gas acts as a liquid is made. However, gas never truly behaves like a real liquid. Surface tension needs to be added in artificially. Viscosity and scale dependence as well as phase transitions might also be studied in the future.

The thermodynamic automata methods presented in this thesis are an alternative to differential equations for modelling of fluid flow and wave propagation in rocks.

Bibliography

- An, L., and Sammis, C. G., 1996, A cellular automaton for the development of crustal shear zones: *Tectonophysics*, **253**, 3-4, 247-270.
- Appert, C., Melayah, A., Pot, V., Rothman, D.H., and Zaleksi, S., 1992, Simulating evaporation in porous media with the lattice gas method: *Proceeding of the international conference on computational modelling in water resources 9*, **2**, 409-416.
- Appert, C., Rothman, D.H., and Zaleski, S., 1991, A liquid-gas model on a lattice: *Physica D* **47**, 85-96.
- Aziz, K., and Settari, A., 1979, *Petroleum reservoir simulation*: Applied Science Publishers.
- Bak, P., and Tang, C., 1989, Earthquakes as a self-organized critical phenomenon: *Journal of Geophysical Research, B, Solid Earth and Planets*, **94**, No.11, 15635-15637.
- Balasubramanian, K., Hayot, F., and Saam, W.F., 1987, Darcy's law from lattice-gas hydrodynamics: *Phys. Rev. A.*, **36**, 2248-2253.
- Barrer, R.M., 1951, *Diffusion in and through solids*: Cambridge University Press, 1-4.
- Baudet, C., Hulin, J.P., Lallemand, P., and d'Humieres, D., 1989, Lattice Gas Automata: A Model for the Simulation of Dispersion Phenomena: *Phys. Fluids A*, **1**, No. 3, 507-512.
- Bean, C. J., and McCloskey, J., 1993, Power-law random behavior of seismic reflectivity in boreholes and its relationship to crustal deformation models: *Earth and Planetary Science Letters*, **117**, 3-4, 423-429.
- Bear, J., 1972, *Dynamics of Fluids in Porous Media*: Published by American Elsevier Company Ltd., 579-582.

Binder, P.M., 1987, Lattice models of the Lorentz gas physical and dynamical properties: *Complex Systems*1, 559-574.

Biot, M. A., 1962, Mechanics of deformation and acoustic propagation in porous media: *J. Appl. Mech.*, **23**, 1482-1498.

Boghosian and Levermore, 1987, *Complex system*, **1**, 1-17.

Boghosian, B. M., 1989, Lattice gases: 295-307. 1989 *Lectures in Complex Systems*. Edited by Erica J. Addision-Wesely, 1990.

Boon, J.P., and Noullez, A., 1989, Lattice gas diffusion and long time correlations: *Word Scientific, Singapore*, 400-408.

Brown, S. R., Scholz, C. H., and Rundle, J. B., 1991, Cellular automaton model of earthquakes: *Eos, Transactions, American Geophysical Union*, **72**, 17, 275.

Burgess, C., and Zaleski, S., 1987, Buoyant mixtures of cellular automata gases: *Complex Systems* 1, 31-50.

Chen, S., Diemer, K., Doolen, D., and Eggert, K., 1991, Lattice gas automata for flow through porous media: *Physica D*, **47**, 72-84

Chen, S., and Matthaeus, W. H., 1987, New cellular automaton model for magnetohydrodynamics: *Phys. Rev. Lett.*, **58**, 1845-1848.

Chen, S., Lee, M., Zhao, K. H., and Doolen, G. D., 1989, A lattice gas model with temperature: *Physica D*, **37**, 42-59.

Chen, S., Matthaeus, W. H., and Klein, L. W., 1988, An analytic theory and formulation of a local magnetohydrodynamic lattice gas model: *Phys. Fluids*, **31**, 1439-1445.

Cheng, E. and Ebner, C., 1993, Dynamics of Liquid-droplet spreading: A monte carlo study: Physical Review B., **47**, No.20, 13808-13811.

Chopard, B., and Droz, M., 1988, Cellular automaton model for heat conduction in a fluid: Phys. Lett. A, **126**, 476-480.

Clavin, Lallemand, P. P., Pomeau, Y., and Searby, G., 1988, Simulation of free boundaries in flow systems by lattice gas models: J. Fluid Mech, **188**, 437-464.

Conway, J., 1982, Winning ways, 2, Chapter25: Academic press.

Darcy, H., 1856. Les Fontaines Publiques De la Ville Dijon, Dalmont, Paris.

de la Cruz, V., and Spanos, T. J. T., 1983. Mobilization of Oil Ganglia: AICHE J., **29**, No. 7, 854-858.

de la Cruz V., and Spanos, T. J. T., 1985. Seismic wave propagation in a porous medium: Geophysics, **50**, 1556-1565.

de la Cruz, V., and Spanos, T. J. T., 1989a. Thermomechanical coupling during seismic wave propagation in a porous medium: J. Geophys. Res., **94**, 637-642.

de la Cruz, V., and Spanos, T. J. T., 1989b. Seismic boundary conditions for porous media, J. Geophys. Res., **94**, 3025-3092.

DeMasi, A., Esposito, R., Lebowitz, J. L., and Presutti, E., 1989, Hydrodynamics of stochastic cellular automata: Commun. Math. Phys, **125**, 127-145.

d'Humières, D., Lallemand, P., and Shimomura, T., 1985, Cellular automata, a new tool for hydrodynamics: Los Alamos National Laboratory Report, LA-UR-85-4501.

d'Humières, D., and Lallemand, P., 1986a, Lattice gas automata for fluid mechanics: Physica A, **140**, 326-335.

d'Humières, D., and Lallemand, P., 1986b, 2-D and 3-D hydrodynamics on lattice gases: *Helv. Phys. Acta*, **59**, 1231-1234.

d'Humières, D., Lallemand, P., and Frisch, U., 1986c, Lattice gas model for 3D hydrodynamics: *Europhys. Lett.*, **2**, No. 4, 291-297.

d'Humières, D., and Lallemand, P., 1987, Numerical solutions of hydrodynamics with lattice gas automata in two dimensions: *Complex Systems* 1, 599-632.

Di, P. L. B., Melayah, A., and Zaleski, S., 1994, Modelling water infiltration in unsaturated porous media by interacting lattice gas cellular automata: *Water Resources Research*, **30**, No.10, 2785-2792.

Dubruue, B., Frisch, U., Hénon, M., and Rivet, J. P., 1991, Low viscosity lattice gases: *Physica D*, **47**, 27-29.

Fried, J. J., and Combarnous, M. A., 1971, Dispersion in porous media: *Adv. Hydrosci.*, **7**, 169-282.

Frisch, U., Hasslacher, B., and Pomeau, Y., 1986, Lattice-gas automata for the Navier-Stokes equation: *Physics Review Letters*, **56**, No. 14, 1505-1508.

Frisch, U., 1991, Relation between the lattice Boltzmann equation and the Navier-Stokes equations: *Physica D*, **47**, 231-232.

Gassman, F., 1951, Über die elastizität poroser medien: *Vierteljahresschrift d. Naturf. Ges. Zurich*, **96**, 1-24.

Grad, H., 1963, *Phys. Fluids*, **6**, 147.

Gunstensen, A.K., and Rothman, D. H., 1991, A lattice-gas model for three immiscible fluids: *Physica D*, **47**, 47-52.

Gunstensen, A.K, 1991, Lattice-Boltzmann studies of two phase flow through three Dimensional models of porous media: MIT Porous flow project. Report No.4, 1-19.

Hardy,J., De Pazzis, O., and Pomeau, y., 1976, Molecular dynamics of a classical lattice gas transport properties and time correction functions: *Physical Review A*, **13**, No.5, 1949-1961.

Hénon, 1992, Implementation of FCHC lattice gas model of the connection machine: *Journal of Statistical Physics*, **68**, Nos. ¾, 353-399.

Holme, R., and Rothman, D. H., 1992, Lattice-gas and lattice-Boltzmann models of miscible fluids: *Journal of Statistical Physics*, **68**, Nos. ¾, 409-422.

Huang, J.I., Chu, Y. H., and Yin, C. S., 1988, Lattice gas automata for modelling acoustic wave propagation in inhomogeneous media: *Geophys. Res. Lett.*, **15**, 1329-1241.

Huang, L. J., 1995, Absorbing boundary and free surface conditions in lattice solid approaches: SEG annual meeting expanded Technical program abstracts with biographies, **65**, 1281-1284.

Janecky, D.R., Chen, S., Dawson, S., Eggert, K. C., and Travis, B. J., 1992, Lattice gas automata for flow and transport in geochemical systems: *Proceedings of the 7th international symposium on water-rock interaction*, **7**, 1043-1046.

Jiao, J., 1996, Doctoral thesis: University of Saskatchewan, Saskatoon, Sk, Canada, 158.

Kuentz, M., Mareschal, J. C., and Lavallee, P., 2000, Numerical estimation of electrical conductivity in saturated porous media with a 2D lattice gas: *Geophysics*, **65**, No.3, 766-772.

Landau, L. D. and Lifshitz, E. M., 1958, *Statistical Physics*: Pergamon Press LTD., London-Paris.

Landau, L. D. and Lifshitz, E. M., 1959, *Fluid mechanics*: Pergamon Press.

Lebowitz, J. L., 1986, Microscopic origin of hydrodynamic equations derivation and consequences: *Physica A*, **140**, 232-239.

Liu, J., Xu, Y., and Wuda, B., 1997, Seismic wave field simulation using phononic lattice solid model: *Oil Geophysical Prospecting*, **32**, No.3, 370-375.

Lundquist, L., and Stewart, C. A., 1992, Using cellular automaton models of plate tectonics to demonstrate consequences of continents on earth vs. purely style lithosphere on Venus; pattern formation and plate distribution: *Eos, Transactions, American Geophysical Union*, **73**, No.43, Suppl., 329-330.

McCauley, J. L., 1987, Chaotic dynamical systems as automata: *Z. Naturforsch*, **42a**, 547-555.

McNamara, G. R. and Zanetti, G., 1988, Use of the Boltzmann equation to simulate lattice –gas automata. *Physical Review Letters*, **61**, No. 20, 2332-2335.

Molvig, K., Donis, P., Miller, R., Myczkowski, J., and Vichniac, G., 1989, Multi-species lattice gas automata for realistic fluid dynamics, in: *Cellular automata and modeling of complex systems*, eds: P. Manneville, N. Boccara, G. Y. Vichinac and R. Bidaux (Springer, Berlin), 206-231.

- Montgomery, D. and Doolen, G. D., 1987, Magnetohydrodynamic cellular automata: Phys. Lett. A, **120**, 229-231.
- Mora, P., 1992, The lattice Boltzmann phononic lattice solid. Journal of Statistical Physics, **68**, Nos. 3/4, 591-609.
- Neumann, J. V., 1966, Theory of self-reproducing automaton: University of Illinois Press.
- Newman, S. p., 1977, Theoretical Derivation of Darcy's Law: Acta. Mech., **25**, 153.
- Oono, Y. and Yeung, C., 1987, A cell dynamic system model of chemical turbulence: J. Stat. Phys., **48**, 593-644.
- Press, W. H., Teukolsky, S. A., Vetterling, W. T., and Flannery, B. P., 1992, Numerical recipes in C, Second edition: Cambridge University Press, 275-287.
- Rothman, D. H., 1987, Modelling seismic P-waves with cellular automata: Geophys. Res. Lett., **14**, 17-22.
- Rothman, D. H., 1990, Macroscopic laws for immiscible two-phase flow in porous media: Results from numerical experiments: J. Geophys. Res, in Press.
- Salomaa, A., 1969, Theory of automata: Pergamon Press.
- Segre, E., and Deangeli, C., 1995, Cellular automaton for realistic modelling of landslides: Nonlinear Process in Geophysics, **2**, No.1, 1-15.
- Steady, S. J., McCloskey, J., Ren, J., Bean, C., and Volant, P., 1995, A 3-D cellular automaton for modelling induced seismicity in the Creighton Mine: Eos, Transactions, American Geophysical Union, **76**, No.46, Suppl. , 354.

Succi, S., 1988, Triangular versus square lattice gas automata for the analysis of two-dimensional vortex fields: *J. Phys. A*, **21**, 43-49.

Succi, S., Benzi, R., and Higuera, F., 1991, The lattice Boltzmann equation: A new tool for computational fluid-dynamics: *Physica D*, **47**, 219-230.

Tipper, J. C., 1997, Modelling carbonate platform sedimentation; lag comes naturally: *Geology (Boulder)*, **25**, No.6, 495-498.

Toffoli, T., 1989, Four topics in lattice gases: ergodicity; relatively; information flow; and rule compression for parallel lattice-gas machines, in: *Discrete Kinetic Theory, Lattice Gas Dynamics and Foundations of Hydrodynamics*. World Scientific, Singapore. 343-354.

Travis, B. J., Eggert, K. G., Chen, S. Y., Doolen, G. D., 1988, Cellular automaton solution for transport in porous and fractured media: *Eos, Transactions, American Geophysical Union*. 69, No.44, Pages 1193.

Udey, N., Shim, D., Spanos, T. J. T., 1999, A Lorentz invariant thermal lattice gas model. *Proc. R. Soc. Lond. A*, **455**, 3565-3587.

Udey, N. and Spanos, T. J. T., 1993, The equations of miscible flow with negligible molecular diffusion: *Transport in Porous Media*, **10**, 1-41.

Waite, M. E., Ge, S., Spetzler, H. and Bahr, D. B., 1998, The effect of surface geometry on fracture permeability; a case study using a sinusoidal fracture: *Geophysical Research Letters*, **25**, No.6, 813-816.

Wapenaar, C. P. A., and Berkhout, A. J., 1989, *Elastic wave field extrapolation*: Elsevier, New York.

Weisbuch, G. 1991, Complex systems dynamics, an introduction to automata networks: Addison-Wesley Publishing Company.

Whitaker, s., 1986, Flow in Porous Media I: A Theoretical Derivation of Darcy's Law: Transport in Porous Media, **1**, 3-25.

Wolfram. S., 1984, Cellular automaton as a model of complexity, review article: Nature, **311**, 419-424.

Wolfram. S., 1986a, Theory and Application of Cellular Automata: World Scientific.

Wolfram. S., 1986b, Cellular automaton fluids 1: Basic theory: Journal of Statistical Physics, **45**, No.3-4, 471-526.

Yang, D., 1997, A thermodynamic automaton and some applications; Doctoral thesis, University of Alberta.

Yang D., Udey, N., and Spanos, T.J.T., 1999, Thermodynamic automaton simulations of fluid flow and diffusion in porous media: Transport in Porous Media, **35**, 37-47.

Zemansky, Mark W., 1957, Heat and thermodynamics: McGraw-Hill book company, Inc.

University of Alberta Library



0 1620 1520 5196

B45570